



Long-term potentiation of the nucleus reuniens and entorhinal cortex to CA1 distal dendritic synapses in mice

Thyna Vu^{1,2} · Radu Gugustea^{1,2} · L. Stan Leung^{1,2} 

Received: 3 December 2019 / Accepted: 31 May 2020 / Published online: 13 June 2020
© Springer-Verlag GmbH Germany, part of Springer Nature 2020

Abstract

The present study investigated the short-term and long-term synaptic plasticity of excitatory synapses formed by the nucleus reuniens (RE) and entorhinal cortex (EC) on the distal apical dendrites of CA1 pyramidal cells. RE-CA1 synapses are implicated in memory involving the hippocampus and medial prefrontal cortex. Current source density (CSD) analysis was used to identify excitatory and inhibitory currents following stimulation of RE or medial perforant path (MPP) in urethane-anesthetized mice *in vivo*. At the distal apical dendrites, RE evoked an initial excitatory sink followed by inhibitory sources at short (~30 ms) and long (150–200 ms) latencies, and often showing gamma (25–40 Hz) oscillations. Both RE-evoked and spontaneous gamma-frequency local field potentials displayed the same CSD depth profile. Paired-pulse facilitation (PPF) of the distal excitatory sink at 20–200 ms interpulse intervals was observed following RE stimulation, generally higher than that following MPP stimulation. Theta-frequency burst stimulation (TBS) of RE induced input-specific long-term potentiation (LTP) at the distal dendritic CA1 synapses, accompanied by reduction of PPF. After TBS of the MPP, the MPP-CA1 distal dendritic synapse could manifest LTP or long-term depression, but the non-tetanized RE-CA1 synapse was typically potentiated. Heterosynaptic potentiation of the RE to CA1 distal synapses may occur after repeated activity of EC afferents, or spread of MPP stimulus currents to coursing RE afferents. The results indicate a propensity of RE-CA1 distal excitatory synapses to show PPF, LTP and gamma oscillations, all of which may participate in memory processing by RE and EC.

Keywords Nucleus reuniens · Temporoammonic pathway · Paired-pulse facilitation · Long-term potentiation · Gamma oscillations · Current source density

Introduction

Two major pathways synapse on the distal apical dendrites of pyramidal cells in the CA1 area of the hippocampus. One comes from the entorhinal cortex (EC), through the perforant path or temporoammonic pathway (Amaral and Witter 1989), and another comes from the nucleus reuniens (RE) (Herkenham 1978; Wouterlood et al. 1990; Dolleman-Van der Weel and Witter 1996; Vertes et al. 2006). The distal dendritic inputs are critical for hippocampal function. The EC (MPP) to CA1 pathway (Amaral and Witter 1989; Witter et al. 1989) provides spatial information to place cells

in CA1 (Brun et al. 2002), which is necessary for spatial memory recall and consolidation (Remondes and Schuman 2004; Brun et al. 2008). The distal dendrites were also activated during performance of oculomotor and manual working memory tasks (Sybirska et al. 2000). A role of the RE has been implicated in learning different aspects of a spatial water maze task (Davoodi et al. 2009; Dolleman-van der Weel et al. 2009), strategy shifting in memory tasks (Cholvin et al. 2013), generalization of fear conditioning (Xu and Sudhof 2013), and in object discrimination but not eye blink conditioning (Eleore et al. 2011). RE is the main intermediary structure connecting the medial prefrontal cortex to the hippocampus (Vertes 2006). Its role was shown to be critical in navigation (Varela et al. 2014; Ito et al. 2015), fear generalization (Xu and Sudhof 2013) and synchronization of slow oscillations (Hauer et al. 2019). RE has been suggested to integrate emotional, motivation, and arousal signals received from other limbic cortices, basal forebrain, and hypothalamus (McKenna and Vertes 2004;

✉ L. Stan Leung
sleung@uwo.ca

¹ Graduate Program in Neuroscience, The University of Western Ontario, London, ON N6A5C1, Canada

² Department of Physiology and Pharmacology, The University of Western Ontario, London, ON N6A5C1, Canada

Vertes 2006), and these integrated signals may help with memory and navigation in the EC and hippocampus.

Synaptic plasticity, in particular long-term potentiation (LTP), has been proposed to be a cellular correlate of memory (Martin et al. 2000; Bliss et al. 2007). Both LTP and long-term depression (LTD) of the distal apical dendrites of CA1 were reported in hippocampal slices *in vitro* (Remondes and Schuman 2002, 2003). However, electrical stimulation of the stratum lacunosum-moleculare (SLM) was expected to activate both the temporoammonic path and RE afferents to CA1, and thus the properties of each pathway could not be distinguished. LTP induced by stimulation of the MPP *in vivo* was reported in anesthetized rats (Leung et al. 1995), and in freely moving rats (Gonzalez et al. 2016). A dual dependence of MPP-induced LTP in CA1 on both NMDA receptors and voltage-gated Ca^{2+} channels was found *in vitro* (Remondes and Schuman 2003) and in behaving rats *in vivo* (Aksoy-Akel and Manahan-Vaughan 2015). There appear to be few studies of LTP of the RE to CA1 synapse in mice. Eleore et al. (2011) did not find LTP after high frequency stimulation of the RE. Bertram and Zhang (1999) reported LTP of thalamo-CA1 responses after midline thalamic stimulation in rats, but their responses did not show the characteristic CA1 distal dendritic excitation following RE activation (Dolleman-Van der Weel et al. 1997; Morales et al. 2007; Hauer et al. 2019).

The distal apical dendrites of CA1 manifest a gamma (30–100 Hz) oscillation, independent of a proximal gamma oscillation (Belluscio et al. 2012; Fernandez-Ruiz et al. 2012; Lasztocki and Klausberger 2014). It was suggested that EC driving and dendritic interneurons are involved in generating the distal dendritic gamma oscillations (Colgin et al. 2009; Lasztocki and Klausberger 2014, 2019; Fernandez-Ruiz et al. 2017). Gamma oscillations are suggested to facilitate sensory processing and memory consolidation (Kay and Freeman 1998; Csicsvari et al. 2003; Fries et al. 2007; Lisman and Jensen 2013).

The purpose of the present study was to investigate the short-term and long-term synaptic plasticity at two distal apical dendritic synapses on CA1 pyramidal cells in mice—RE to CA1 and EC to CA1 by medial perforant path (MPP) stimulation. We recorded laminar profiles of field potentials using a multichannel electrode in urethane-anesthetized mice, and applied current source density (CSD) analysis to isolate the responses in CA1 and dentate gyrus (DG). The CSD profile of evoked distal apical dendritic excitation was similar to that of the spontaneous distal dendritic gamma oscillations. We reported a relative ease of inducing paired-pulse facilitation (PPF) and gamma oscillations at the RE to CA1 synapse, as compared to the EC-CA1 synapse. LTP of the RE to CA1 synapses was readily induced by tetanic stimulation of the RE, and unexpectedly, also by tetanic stimulation of the MPP.

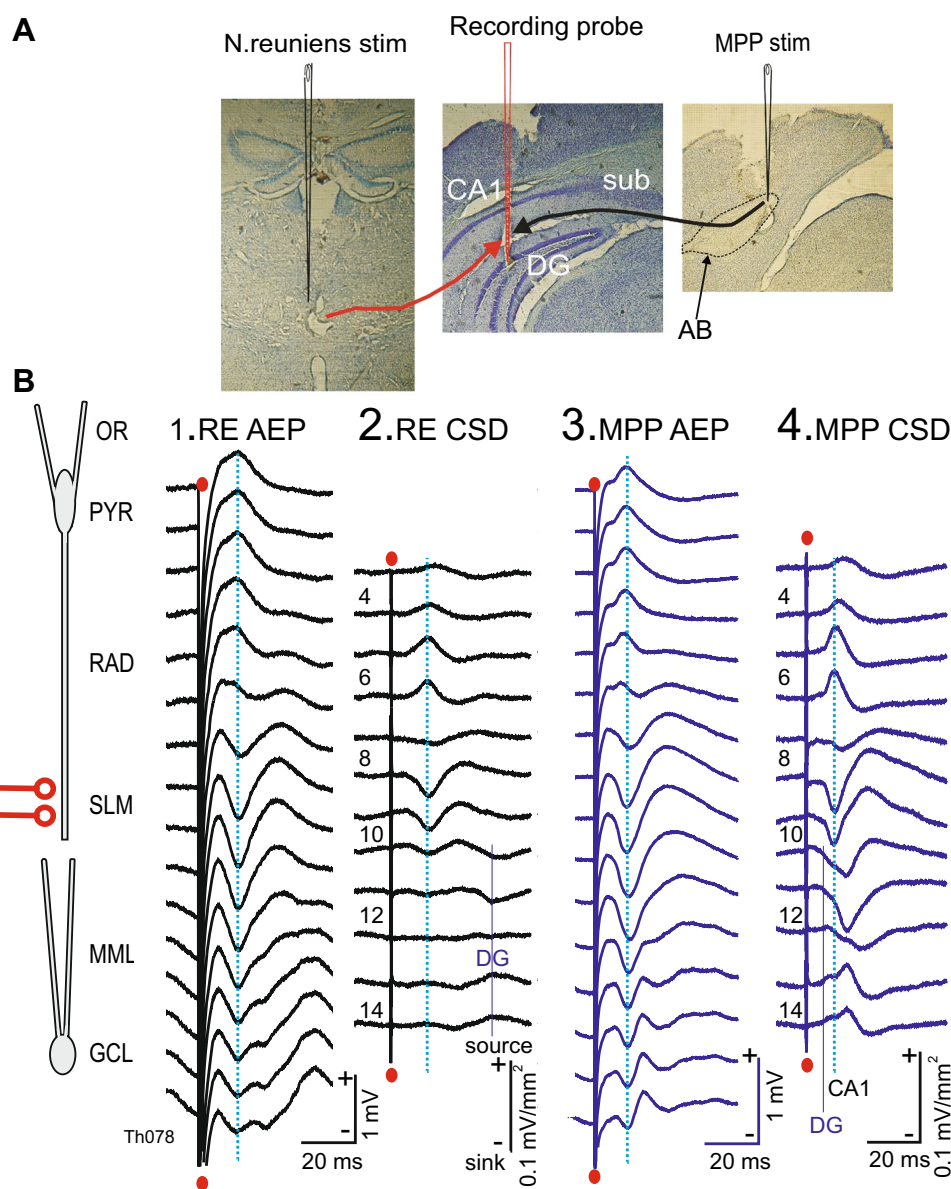
Methods

Forty mice (20–35 g) were used. Wildtype mice were derived after backcrossing of 129/SvEv with C57BL/6 mice (Al-Onaizi et al. 2016). Mice were housed in standard cages in a temperature-regulated environment with a 12:12 h light/dark cycle, with lights on at the 7th h, and had *ad libitum* access to food and water. Experiments were conducted during the day (10–22 h). All experiments complied with the Animals for Research Act regulations of the province of Ontario and were approved by the Western University Animal Care and Use Committee.

Mice were anaesthetized with 1.25 g/kg *i.p.* of urethane solution and supplemented by 5–10% of the initial dose as needed (Hutchison et al. 2009). Atropine methyl nitrate (7.5 mg/kg, *i.p.*) was injected to reduce salivation. A rectal thermometer monitoring system was used to maintain body temperature at 36–37 °C throughout the experiment. The skull was exposed, bregma and lambda were placed on a horizontal plane, and small skull holes were drilled based on the stereotaxic atlas of Franklin and Paxinos (2008). A silicon multi-channel recording electrode was lowered vertically into the brain at posterior (P) 3.2 mm and lateral (L) 2.8 mm with respect to bregma, to record from CA1 (Fig. 1a). The dorsal blade of dentate gyrus (DG) was also recorded in about half the animals. Stimulating electrode (125 μm diameter Teflon-insulated wire except at the cut tip) was placed, in different experiments, in (1) medial perforant pathway (MPP) at P4.1, L2.3, and ~1.3 mm ventral (V) from the skull surface, (3) nucleus reuniens (RE) at P0.8, L0, V ~4.4 mm, and/or (3) CA1 stratum radiatum (RAD) at P3.2, L2.5, V ~2 mm. The depth of a stimulating electrode was optimized to give the lowest threshold in the track (using cathodal currents). Depth of the recording electrode (750 μm span) was placed in different experiments to include either the DG or CA1 stratum oriens. Two screws were then secured onto the skull above the frontal cortex and cerebellum to serve as stimulus anode and recording ground, respectively.

Silicon recording probes were purchased from NeuroNexus, Ann Arbor, MI; the probes had 16 recording sites spaced 50 μm apart on a vertical shank (Model #: A1 \times 16-5 mm-177-16; CM type was also used). Signals from the 16-channel recording probe were amplified 200–1000 \times by a TDT (Tucker-Davis Tech, TDT) headstage, a 16-channel Medusa preamplifier (band pass filter between 2.2 Hz and 7.5 kHz) and fed by optic wires to TDT digital processors (RA16 Base Station). Signals were digitized at 6.1–24.4 kHz by TDT real-time processors and custom-made software. Stimulus pulses (0.2 ms duration) were delivered through a photo-isolated stimulus isolation unit (PSIU6, AstroMed/Grass Instrument). Single sweeps

Fig. 1 Schematic of stimulation and recording and representative average evoked potentials (AEPs) and current source density (CSD) time transients following stimulation of the nucleus reuniens (RE) or medial perforant path (MPP). **a** Thionin-stained sections showing location of stimulating electrode (after lesion) at the RE (leftmost) and medial part of the angular bundle (AB, rightmost) to activate the MPP; recording probe was inserted into CA1a near the subiculum (sub). **b** Schematic CA1 pyramidal cell and dentate gyrus granule cell (left), showing AEPs ($n=24$ sweeps) and CSDs following stimulation of RE at $300 \mu\text{A}$, at $1.5 \times$ threshold intensity (columns 1 and 2), or MPP stimulation at $60 \mu\text{A}$, at $2 \times$ threshold intensity (columns 3 and 4). Excitation of the distal apical dendrites was characterized by negative potentials (and current sinks) at stratum lacunosum-moleculare (SLM) and positive potentials (and current sources) at stratum radiatum (RAD). Other layers are: OR stratum oriens, PYR stratum pyramidale, MML middle molecular layer, GCL granule cell layer. Filled circle indicates stimulus artifact



of evoked potentials and the average ($n=4$) were stored; repetition rate was 0.1 Hz. A one-dimensional $CSD(z,t)$ as a function of depth z and time t was calculated by a second-order differencing formula (Leung 2010):

$$CSD(z,t) = \sigma[2\Phi(z,t) - \Phi(z + n \Delta z,t) - \Phi(z - n \Delta z,t)] / (n \Delta z)^2, \tag{1}$$

where $\Phi(z,t)$ is the potential at depth z and time t , Δz is the spacing ($50 \mu\text{m}$) between adjacent electrodes on the 16-channel probe, and $n=2$ (2-step CSD) was used unless otherwise noted. The conductivity σ was assumed to be constant and CSDs were reported in units of V/mm^2 .

Mice were grouped according to the main experiments intending to induce LTP or LTD at the RE or MPP to CA1 pathway using theta-burst stimulation (Table 1). Baseline

electrophysiological measures were obtained before TBS, including: (1) threshold intensity (T), operationally defined as the minimal stimulus intensity that evoked a detectable response in the AEP ($n=4$ sweeps); (2) input–output relation of the RE and MPP response was determined using $1-5 \times T$ stimulus intensity, to a maximum of $600 \mu\text{A}$; (3) paired-pulse responses at interpulse interval (IPI) of 50 or 200 ms, or in some experiments, across the IPI range of 10–200 ms, and (4) spontaneous local field potentials.

Cathodal, paired pulses of 50 or 200 ms IPI, were applied to one stimulus electrode (RE or MPP) to study the time course of LTP or LTD. Maximal RE monitoring stimulus intensity was set at $500 \mu\text{A}$, which could be $1-1.5 \times T$; MPP was set at $2 \times T$ stimulus intensity. A stable baseline was defined to show a SEM/mean ratio of the sink slopes of <0.10 (at the electrode with the maximal

Table 1 Number of animals that contributed to data, categorized as different groups

Group	Animals	With RE stimulus	With MPP stimulus
Nucleus reuniens LTP	7	7	5
Nucleus reuniens—no LTP	1	1	1
Nucleus reuniens other	5	5	0
RE and MPP pilot studies	6	Excluded	Excluded
Medial perforant path LTP	7	3	7
Medial perforant path LTD	6	6	6
Medial perforant path other	8	3	8
Total	40	25	27

Animals were grouped under long-term potentiation (LTP), long-term depression (LTD), or other following the two structures stimulated—nucleus reuniens (RE) and medial perforant path (MPP). Theta burst stimulation (TBS) was used to induce LTP of the RE to CA1 synapse, and either LTP or LTD of the MPP to CA1 synapse. Baseline electrophysiological data (laminar profiles, input–output relation, paired-pulse ratio, spontaneous local field potentials) were collected before TBS. Only baseline data were collected in “other” experiments

sink) for 6 average CSDs over 30 min. After attaining a stable baseline, theta-burst stimulation (TBS) was delivered. Another stimulus (MPP, RE or RAD), served as a non-tetanized, control pathway. TBS consisted of 10 trains of 10 bursts, with each burst consisting of 10 pulses at 100 Hz; bursts were delivered at 5 Hz (every 200 ms), and trains at every 10 s; pulse intensity was at $2\text{--}4 \times T$ of a single-pulse response. AEPs were recorded at 2 min post-TBS, and then regularly at 5 min intervals starting at 5 min post-TBS, until 120 min post-TBS. Experiments ($< 10\%$ of total) in which responses became unstable after TBS were excluded from LTP/LTD analysis. The criterion of instability was a shift of peak CSD responses by more than one channel, or a $> 30\%$ change of normalized response within 10 min at > 5 min post-TBS.

At the end of the experiment, the sites of the stimulating electrodes were lesioned by passing 0.5 mA current for a duration of 0.5 s, three times with an interval of 10 s between pulses. The mouse was then intracardially perfused with 50 mL of saline followed by 25 mL of 4% formaldehyde solution. The brain was removed from the cranium and placed in 4% formaldehyde solution for a minimum of 72 h prior to sectioning by a freezing microtome. The tip of each stimulating electrode was identified in 40- μ m thick coronal sections stained with thionin (Fig. 1a). The track of the recording probe could be readily discerned in most brain sections, but the exact depth could not be determined. The depth of recording was determined by electrophysiological criteria. With near-horizontal layers of CA1, RAD stimulation evoked a proximal apical dendritic sink in CA1 stratum radiatum (RAD), accompanied by a major source in the pyramidal cell layer (PYR), and a minor source in SLM (Leung et al. 2008; Law and Leung 2018). Distal dendritic excitation of CA1, evoked by MPP or RE stimulation, showed a maximal sink at SLM, accompanied by a source in RAD.

For analysis of paired-pulse ratio (PPR) and LTP, the main analysis used the maximal slope of the excitatory sink recorded at the depth with the maximal sink, i.e., SLM for the monosynaptic CA1 response to MPP or RE. Maximal sink slope was defined as the largest negative slope within a 1-ms interval during the rising phase of the sink. In addition, the peak of the excitatory sink response was measured as the deviation from a pre-stimulus baseline. Slope of the excitatory sink (or AEP) is optimal for measuring an early evoked response, here an excitatory postsynaptic current (or potential). A sink peak measure may be contaminated with delayed inhibitory currents and other polysynaptic events, but may register a larger excitatory current/potential.

$E1$ was defined as the maximal slope of the excitatory sink evoked by the 1st pulse, and $E1$ peak referred to the excitatory sink peak. PPR or $E2/E1$ ratio was defined as the maximal slope of the excitatory sink evoked by the 2nd pulse ($E2$) divided by that evoked by the 1st pulse ($E1$). PPR occurs when $E2/E1 > 1$. For each experiment, $E1$ slope was normalized by the average $E1$ slope during a 30 min baseline. In order to reduce variability, running average of 3 consecutive time points was made during baseline (before TBS), and also after TBS. Running averages did not cross time 0, which was defined as the time of TBS delivery. LTP was assessed by the time course of normalized $E1$ slope. $E1$ peak was measured at a fixed time after the stimulus, and the time instant was at the peak sink during baseline. $E1$ peak was normalized and subjected to time course analysis like the $E1$ (slope). Statistical analysis of potentiation used the 3-point running averages of the normalized data, which gave 4 time points during baseline ($- 25$ to $- 10$ min) and 23 time points ($5\text{--}115$ min) post-TBS. $E1$, $E2$ and $E2/E1$ changes were also assessed by the average values in 5 time periods of 30 min each—baseline ($- 30$ to 0 min), LTP1 ($0\text{--}30$ min post-TBS), LTP2 ($30\text{--}60$ min), LTP3 ($60\text{--}90$ min) and LTP4 ($90\text{--}120$ min). Other than giving a more reliable

estimate because of larger number of sweeps, a 30-min block also averaged across different brain states. Rodents under urethane anesthesia were shown to cycle between slow-wave (SW) state, with high power < 3 Hz, and theta (with high 3–7 Hz power) states (Clement et al. 2008). A block of 30 min is expected to average more than one cycle of SW and theta states (Law and Leung 2018). The MPP to SLM $E1$ was not statistically different between SW and theta states during baseline (Leung and Peloquin 2010). Pilot data ($n=4$ mice) also indicated that MPP-SLM $E1$ was not significantly different between SW and theta states at a fixed time after TBS of the MPP.

In many experiments, about 60 min of spontaneous local field potential (LFP) activity was recorded during baseline, before TBS. The CSD activity derived from these LFPs, was subjected to auto- and cross-power spectral analysis (Leung et al. 1982). LFPs were sampled at 6.104 kHz, and segments of 8192 points (1.34 s) from 2 channels were analyzed for autopower, phase and coherence (squared coherence). A segment of spontaneous LFP activity at a SLM electrode was classified as theta and SW states—theta state showed peak power at a theta frequency (2.98–6 Hz) and SW state showed peak power at 1–2 Hz with no theta peak. Spontaneous LFP segments with theta peaks at 3.72 and/or 4.47 Hz (50–80 segments per mouse) were selected for analysis of gamma activity with depth. In some mice, depth profiles of gamma activity during SW were also analyzed. In the analysis of depth profile in relation to SLM gamma, the gamma amplitude at each depth was the peak amplitude (square root of the autopower) multiplied by the cosine of the cross-spectral phase at each depth.

Data are shown as mean \pm standard error of the mean (SEM). Data from two groups were compared using paired- or unpaired t test, as appropriate. Repeated measures (RM) analysis of variance (ANOVA) was used for statistical analysis of the normalized data. $P < 0.05$ was considered statistically significant. If a significant main or interaction effect was found, Newman–Keuls post hoc tests were applied.

Results

Distal dendritic excitation of CA1 by stimulation of RE

Stimulation of the RE in the mouse, confirmed by histological examination (Fig. 1a), evoked a dipole response in hippocampal CA1, consisting of a positive AEP peak at the alveus and pyramidal cell layer (PYR) of CA1, accompanied by a negative AEP peak near SLM (Fig. 1b). A population spike was not observed in CA1 or DG after RE stimulation of up to 600 μ A; however, CA1 population spikes could appear when the stimulating electrode passed within 1 mm

of the ventral hippocampal commissure, about 2.2 mm above RE. CSD analysis revealed that the RE-evoked dipole field was generated by a current sink at the distal apical dendrites at SLM, concomitant with a current source at the proximal apical dendrites or RAD (Fig. 1b2). The current sink was interpreted to result from excitatory inward currents at the distal apical dendrites (SLM), followed by the passive exit of the intracellular currents at the proximal apical dendrites, giving a current source at RAD. The onset of the SLM excitatory sink following single-pulse RE stimulation was 9.15 ± 0.42 ms (mean \pm SEM, $n=25$). The minimal RE threshold of evoking a CA1 response was ~ 200 μ A; the average was 314 ± 22 μ A ($n=25$). These characteristics of CA1 response to RE stimulation were similar to those reported previously in rats by Dolleman-Van der Weel et al. (1997).

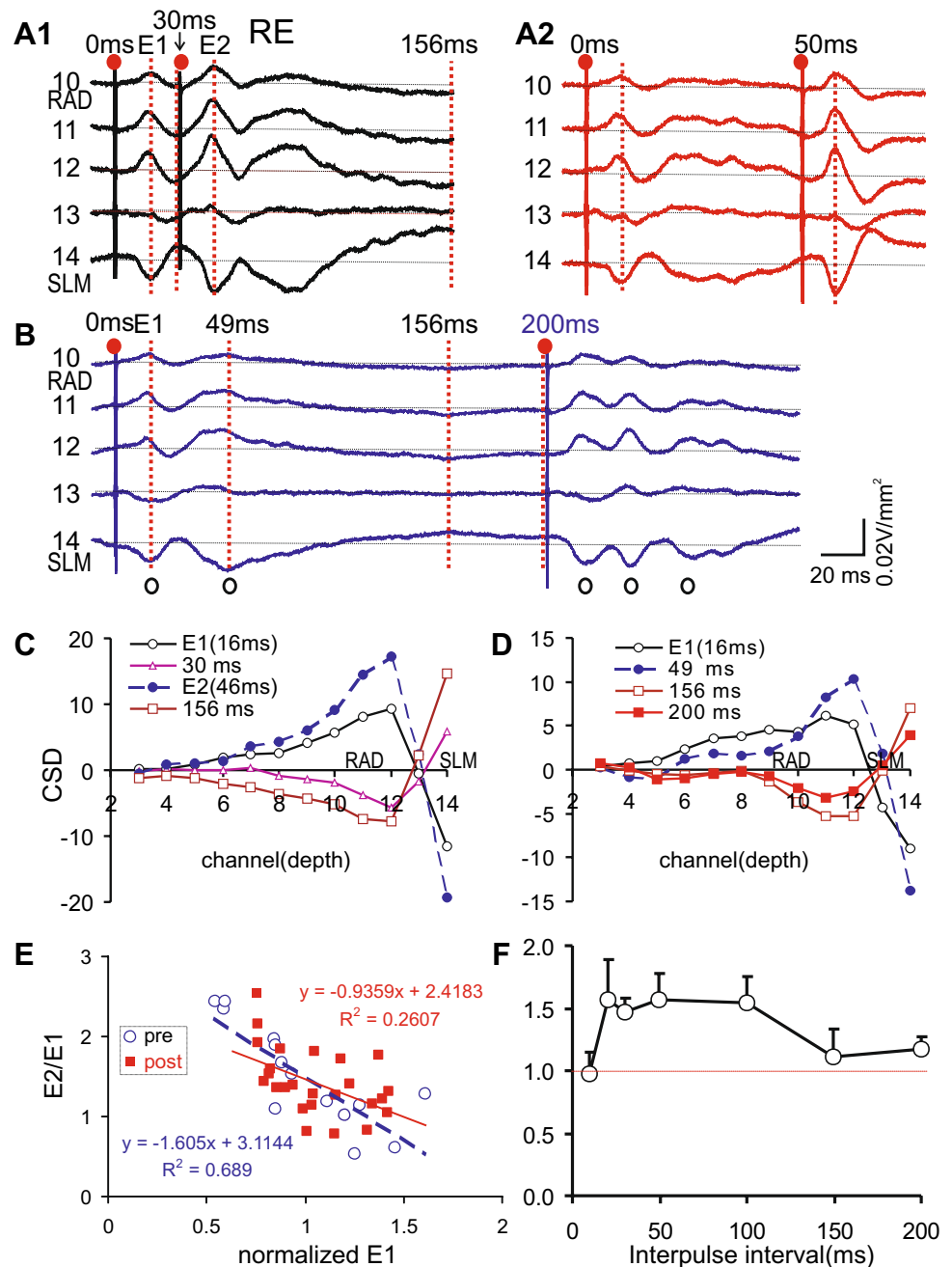
RE stimulation typically evoked no distinct CSDs in the DG at < 9 ms. At a long latency (> 10 ms), a low-amplitude dipole with a sink at the outer molecular layer (OML) of DG, accompanied by a ventral source, was observed in the example illustrated (Fig. 1b). In a group of 13 mice in which both CA1 and DG were recorded, the sink at DG molecular layer started at 11.6 ± 1.05 ms ($n=13$), significantly later than the onset of the CA1 SLM sink at 8.9 ± 0.4 ms [$t(12)=2.37$, $P=0.035$, paired t test].

Paired-pulse stimulation of RE typically yielded PPF ($E2/E1 > 1$) at interpulse intervals (IPIs) of 20–200 ms (Fig. 2a, b, f). The average PPF was similar at 20–150 ms IPI, with lower values at 10 ms and 200 ms IPI (Fig. 2f). PPR ($E2/E1$ ratio) generally decreased as the 1st pulse response $E1$ increased, which could be described by a linear graph (Fig. 2e, plotted for $1.25 \times T$ stimulus intensity and 50 ms IPI, using averages of 4 sweeps). PPR as a function of stimulus intensity (available from $1-3 \times T$ stimulus intensity) for RE stimulation also decreased with increasing stimulus intensity (data not shown).

In about half the animals, a single stimulus pulse delivered to the RE evoked more than one sink peak (open circles in Fig. 2b), with the interval between peaks measuring 20–40 ms. Some responses showed three peaks (e.g., 2nd pulse response in Fig. 2b). The 2nd pulse $E2$ peak showed the same CSD depth profile as the first $E1$ peak (Fig. 2a–c), with SLM sink and RAD source, except $E2$ peak was larger than $E1$ peak (Fig. 2c).

At long latencies (150–200 ms) following 1st or 2nd RE stimulation pulse, a CSD depth profile with SLM source and RAD sink was observed (156 or 200 ms labeled traces in Fig. 2c, d). This reversal of the initial SLM sink to source at 150–200 ms latency suggests a late postsynaptic inhibition at the distal apical dendrites. Long-latency inhibition of the distal dendrites could be mediated by feedforward activation of neurogliaform cells (Capogna 2011). A SLM source, with an accompanying RAD sink, was also observed at a shorter latency following the initial SLM sink (30 ms latency

Fig. 2 CSD profile of responses following paired-pulse stimulation of nucleus reuniens (RE) in a representative mouse. **a1** CSD temporal traces recorded at 5 channels around stratum lacunosum-moleculare (SLM) following RE paired-pulses at interpulse interval (IPI) of 30 ms (**a1**) or 50 ms (**a2**); 2nd pulse response (*E2*) was larger than 1st pulse response (*E1*). **b** Responses to RE stimulation at 200 ms IPI; open circle indicates SLM sink peaks, vertical dotted lines indicates times of depth profile shown in **d**. **c** CSD depth profile at different times indicated in panel **a**; the profile at 30 ms or 156 ms latency was a mirror image of that at 16 ms or 46 ms. **d** CSD profiles at times indicated in panel **b**. **e** Relation of *E2/E1* (slope ratio) plotted with *E1*. Open circles, 5–70 min pre-tetanus; filled rectangles, 2–120 min post-tetanus. All *E1* normalized by the pre-tetanus (pre) average linear regression lines with R^2 shown for pre- and post-tetanus conditions. **f** Group data of *E2/E1* ratio (of slope measures) following RE stimulus. At each data point $n=3-4$ mice, except at 50 ms ($n=7$), and 200 ms ($n=14$); error bar indicates SEM



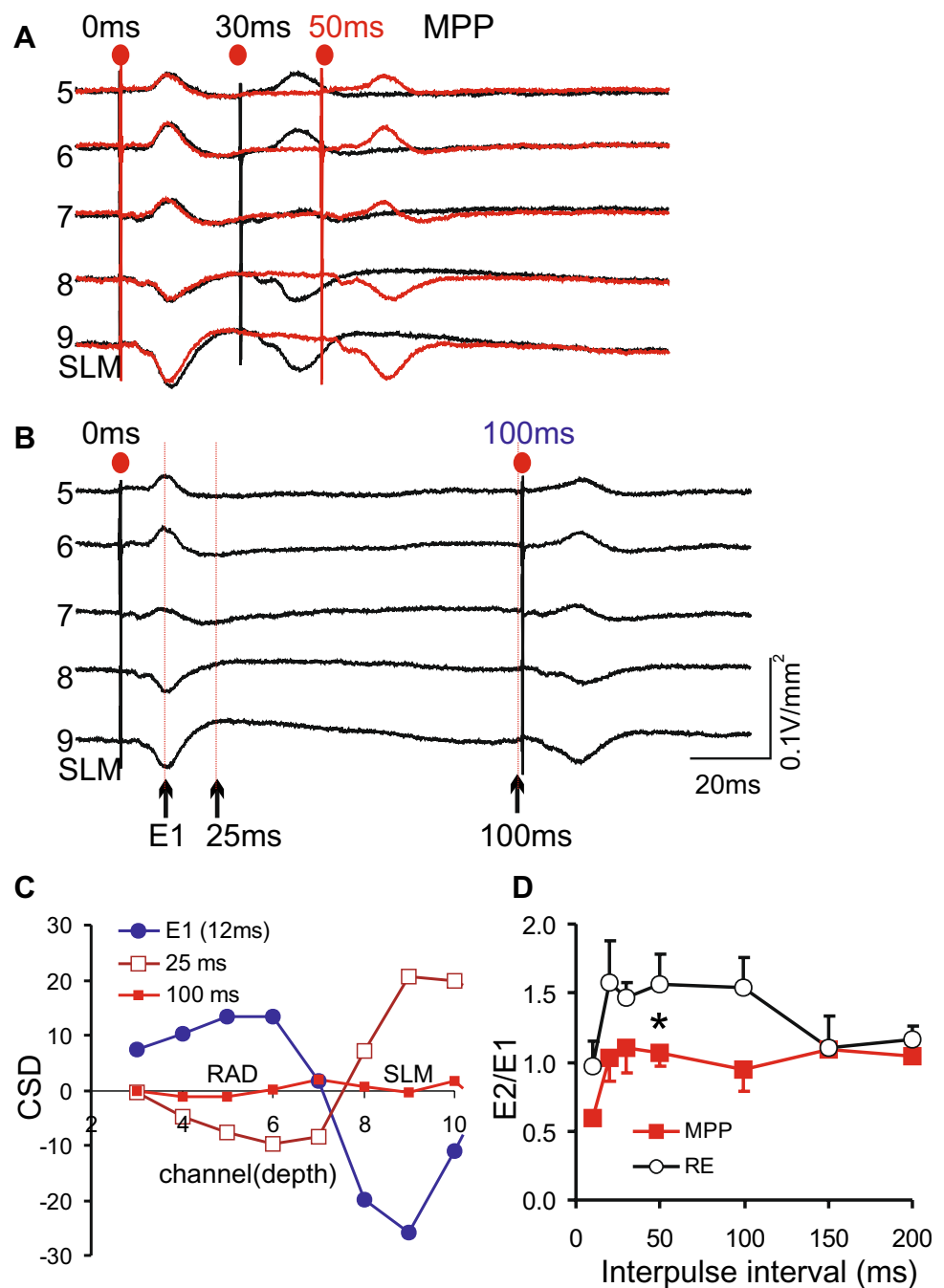
trace in Fig. 2c), suggesting an early postsynaptic inhibition at the distal dendrites. Activation of perforant-path associated interneurons could provide an early GABA_A-receptor mediated inhibition of the distal dendrites (Laszotzci and Klausberger 2014, 2019).

In summary of this section, stimulation of the RE in mice evoked a clear distal dendritic (SLM) sink in CA1 accompanied by a mid-apical dendritic source in RAD. The early distal dendritic sink was followed by a subsequent source, and sometimes oscillation of source-sinks in the gamma frequency range. Delayed, presumably polysynaptic, activation of the DG was also observed.

Distal dendritic excitation of CA1 by stimulation of MPP

Similar to that following RE stimulation, the initial voltage profile in CA1 following MPP stimulation was SLM negative and RAD positive (Fig. 1b3). CSD analysis revealed a SLM current sink and a RAD source (Fig. 1b4, 3a–c). The onset latency of the SLM sink following MPP stimulation was 5.3 ± 0.4 ms ($n=27$), following $2 \times$ threshold stimulation, with threshold of the MPP determined as 31.2 ± 2.8 μ A ($n=27$). At 25–100 ms latency, a reversed pattern of CSDs, with SLM source

Fig. 3 CSD profile of responses following paired-pulse stimulation of medial perforant path (MPP) in a representative mouse. **a** Overlaid responses to paired-pulse stimulation at 30 ms and 50 ms interpulse intervals (IPIs) from selected channels including SLM and RAD. **b** Response to paired pulses at 100 ms IPI. **c** CSD depth profile at different times indicated in panel **b**. **d** Group data of $E2/E1$ ratio (of slope measures) following MPP and RE stimulation. At each data point $n=3-5$ mice, except at 50 ms ($n=7$), and 200 ms ($n=14$); error bar indicates SEM



and RAD sink was observed (Fig. 3c), which suggests inhibition of the SLM. However, oscillation at the gamma frequency was not observed after MPP stimulation. MPP stimulation also activated a short-latency current sink at the middle molecular layer (MML) of the DG (ch10–11 in Fig. 1b4), estimated to start at 3.4 ± 0.6 ms ($n=15$; only about half the mice had recordings in DG). The small DG sink in relation to the CA1 SLM sink (Figs. 1b4, 5a) was a result of optimizing the CA1 response. An optimal

stimulus site was found at the ventral medial part of the angular bundle (Fig. 1a right).

MPP evoked CA1 distal dendritic sink showed paired-pulse depression, or PPR < 1, in the 10–100 ms IPI range for the example given (Fig. 3a, b). As a group, the $E2/E1$ ratio versus IPI plot for MPP stimulation was not statistically different from unity, except for paired-pulse depression at 10 ms IPI. The average $E2/E1$ ratio (recorded in SLM) following MPP stimulation was smaller than that

following RE stimulation (Fig. 3d), and the difference in $E2/E1$ ratio was statistically significant at 50 ms IPI ($P < 0.05$, paired Wilcoxon, $n = 7$), but marginally non-significant at 200 ms IPI ($P = 0.06$, paired Wilcoxon, $n = 14$).

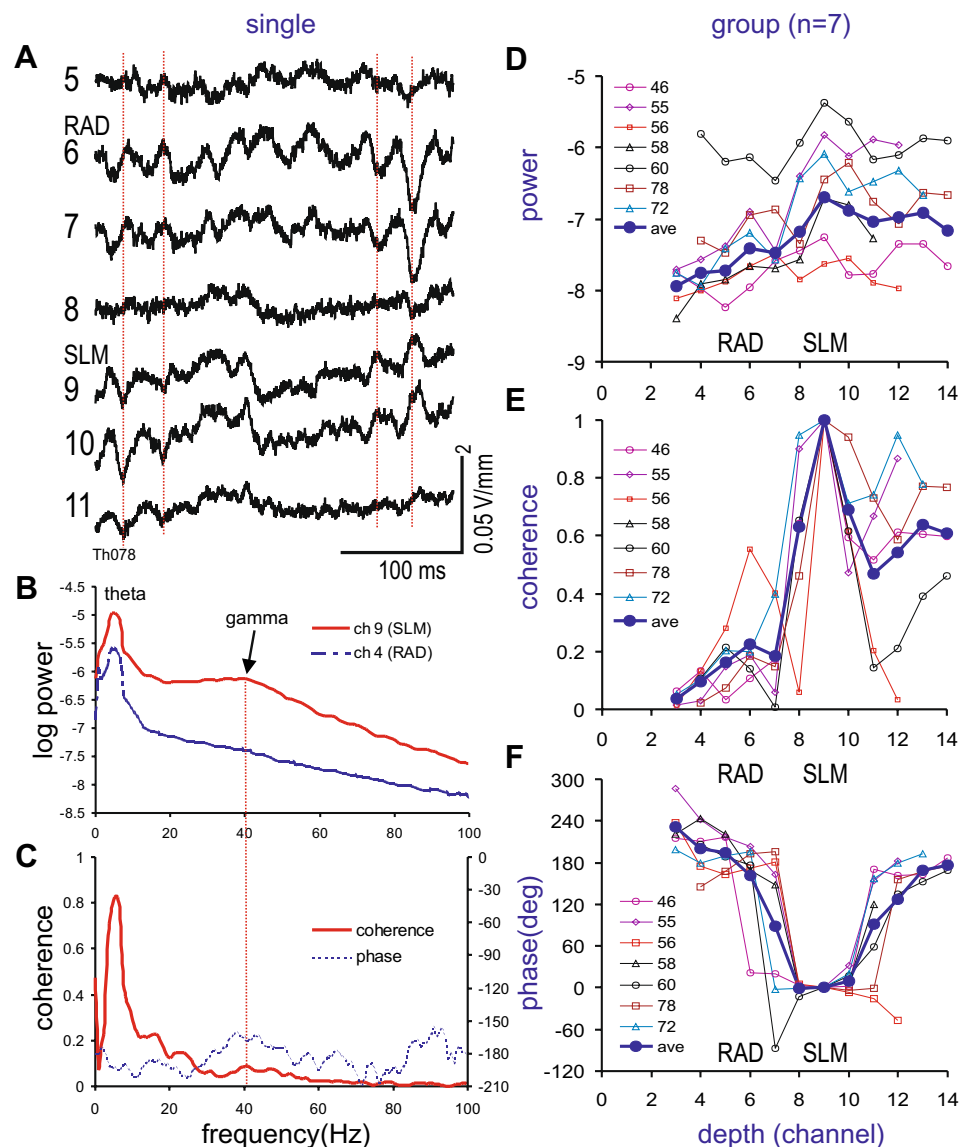
In summary, MPP stimulation also evoked an early excitatory sink followed by a late source in SLM. The MPP stimulus threshold, sink onset latency, and PPR were considerably smaller than the respective measure for RE.

CSDs of spontaneous LFPs revealed a distal dendritic dipole

The spontaneous CSD activity in hippocampal CA1 showed 20–50 Hz oscillations, with source-sink polarity reversal from RAD to SLM. Since gamma activity was larger during theta than non-theta activities (Leung et al. 1982; Bragin et al. 1995), segments of LFPs with clear rhythmic theta

activity were selected for spectral analysis (Fig. 4a). Similar CSD profiles reported below were also found when gamma during non-theta states were analyzed. In a representative mouse, cross-spectral analysis revealed higher gamma power at SLM than at RAD (Fig. 4b), with the gamma peak squared coherence of ~ 0.2 and $\sim 180^\circ$ phase shift between LFPs from RAD and SLM (Fig. 4c). In a group of animals, using LFPs at different depths in relation to LFPs at SLM yielded a near-complete phase reversal in RAD-SLM electrode pairs (separated by 150 μm), with phase $161.7^\circ \pm 24.0^\circ$ ($n = 7$) and coherence 0.22 ± 0.06 ($n = 7$). The power and coherence peaks in SLM and RAD, a phase reversal, and a coherence minimum between SLM and RAD, are consistent with a major generation of the spontaneous gamma oscillations at the distal dendritic layers in CA1. Another gamma power/coherence peak, accompanied by near 180° phase shift was also observed in the DG, ventral to SLM, suggesting that

Fig. 4 CSDs of the spontaneous gamma activity reversed between stratum radiatum (RAD) and stratum lacunosum-moleculare (SLM). **a** Spontaneous gamma CSDs at selected channels (ch) of a representative mouse (same mouse shown in Figs. 1 and 5). **b** Logarithmic power spectra of spontaneous CSDs from a RAD electrode (ch 4) and a SLM electrode (ch 9), and **c** cross-spectra shown as phase (degrees) and coherence. **d–f** Group data, aligned by putative SLM channel, shown as the average (thick line) and individual thin lines for each of 7 mice, average of 7 mice except at ch 3, 12, 13 and 14 ($n = 5, 6, 4$ and 3, respectively). **d** Power, **e** coherence and **f** phase at 40 Hz (gamma power peak) as a function of depth. Phase and coherence were estimated with reference to the SLM channel, thus phase = 0° and coherence = 1 at the SLM channel. Power and coherence peak appeared at SLM, with smaller peaks at RAD (ch 6), and DG (ch 13), with RAD and DG gamma phase shifted by $\sim 180^\circ$ from the SLM gamma



gamma was also generated in the DG. When the depth profile of the RE-evoked CSD (at the $E1$ peak) was compared with that of the amplitude of the spontaneous gamma CSD (Methods), the correlation of evoked CSD with spontaneous CSD depth profiles was 0.87 ± 0.05 ($n = 7$ mice, over 7 depths from ch4 to ch10 in Fig. 4d; evoked CSD profiles were not shown). The high correlation indicates that the evoked and spontaneous profiles were almost identical.

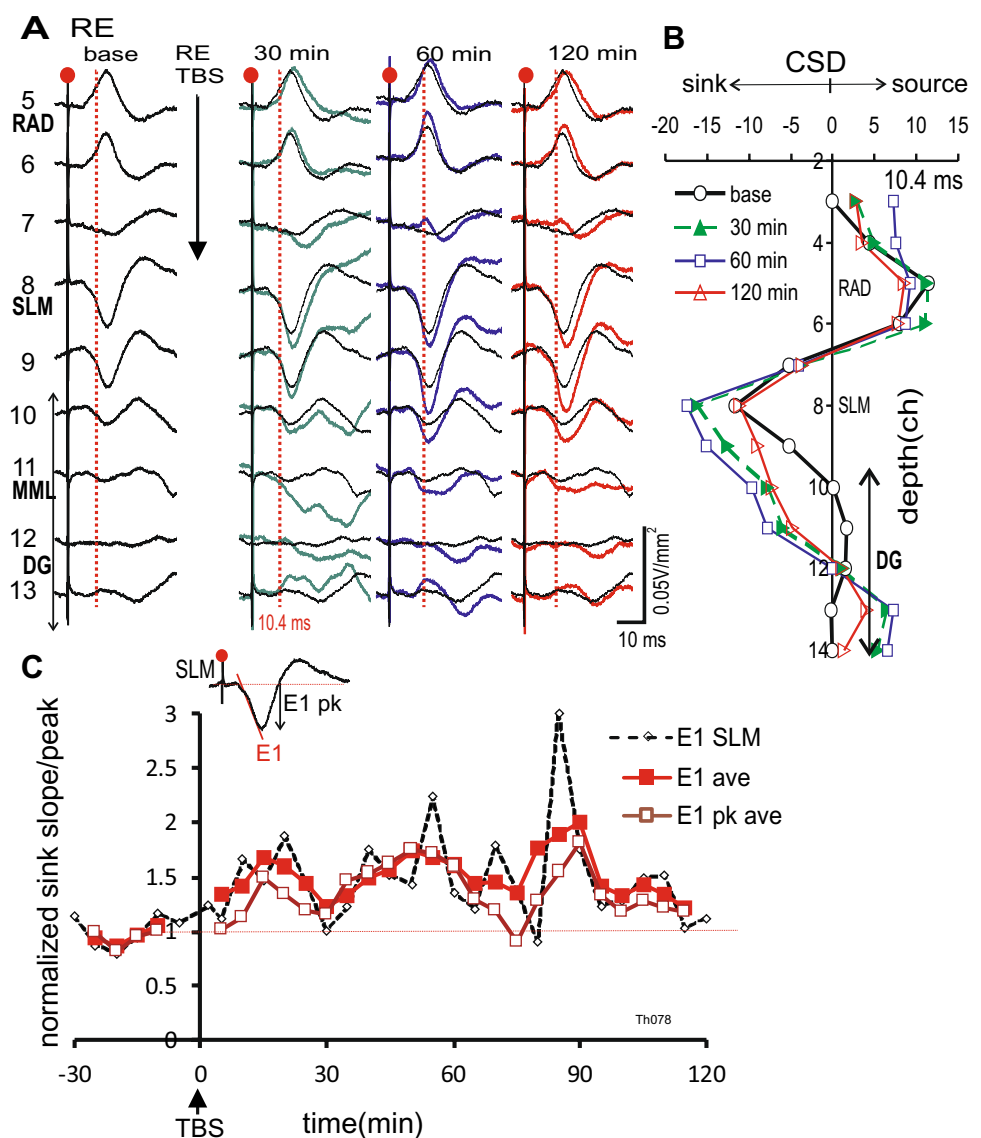
LTP induced by theta burst stimulation (TBS) of RE

Paired-pulse responses to RE stimulation (at $1\text{--}2 \times T$ intensity) were recorded for at least 30 min before, and 120 min after TBS of the RE. In a group of 7 mice selected for LTP of the RE to CA1 synapse (RE-LTP group), test pulses were delivered at $400 \pm 49 \mu\text{A}$ ($n = 7$; $\sim 1.4 \times T$ intensity), and TBS pulse intensity was $436 \pm 32 \mu\text{A}$ ($n = 7$; $\sim 1.7 \times T$ intensity).

As illustrated by a representative example, RE-TBS induced an increase in the 1st pulse excitatory sink at SLM, and its accompanying source at RAD (Fig. 5a top traces). The 1st pulse SLM sink slope ($E1$), normalized by the average pre-stimulus $E1$, was increased for 120 min after TBS, as judged by the measures recorded every 5 min, or by a running average of 3 points (Fig. 5c). The running average of the $E1$ peak at SLM also showed potentiation after TBS (Fig. 5c).

To observe the spatial changes of CSDs, a CSD depth profile was constructed from the grand average of a 30-min block (each with 24 sweeps), and there were 5 blocks—one baseline (-30 to 0 min), and 4 blocks post-TBS named LTP1 ($0\text{--}30$ min), LTP2 ($30\text{--}60$ min), LTP3 ($60\text{--}90$ min), and LTP4 ($90\text{--}120$ min post-TBS). The CSD profiles were constructed at a fixed time instant, about half-way to the SLM sink peak (at 10.4 ms latency in Fig. 5b). During baseline, the CSD profile showed a dipole in CA1, with

Fig. 5 Long-term potentiation of the RE-evoked CA1 distal dendritic responses following a RE tetanus, shown in a representative mouse. Theta burst stimulation (TBS) was delivered to RE at time 0. **a** Average CSD responses ($n = 24$ sweeps) following first RE pulse ($300 \mu\text{A}$) for electrode channel (ch) 5–13, spanning CA1 stratum radiatum (RAD at ch 5) to dentate gyrus (DG) granule cell layer (at ch 13), shown for baseline (base, before TBS at -30 min to -5 min), 5–30 min post-TBS (labeled as 30 min), 30–60 min post-TBS (labeled as 60 min), and 90–120 min post-TBS (labeled as 120 min); post-TBS response (thick trace) is overlaid on baseline (thin trace). Vertical line indicates 10.4 ms latency, at the mid-rising phase of the RE-SLM sink response. **b** CSD depth profiles (averaged for 30 min) at a fixed time instant (10.4 ms latency after RE stimulus), averaged for 4 periods of time (baseline, 30, 60 and 120 min). **c** Time plot shows normalized slope of the 1st pulse excitatory sink ($E1$) at ch 8 stratum lacunosum-moleculare (SLM), 3-point running average (ave) of $E1$ slope (solid rectangles) and $E1$ peak (open rectangles) at SLM



SLM sink and RAD source; CSDs in the DG were of low-amplitude (Fig. 5b). All post-TBS periods (LTP1 to LTP4) showed a larger SLM sink [at channel (ch) 8 in Fig. 5b] than baseline. Somewhat surprisingly, a DG dipole was seen only post-TBS, and not during baseline; the DG dipole had sinks at ch10–11 (inferred to be DG OML), concomitant with sources at ch13–14 (Fig. 5b).

In a group of 7 mice selected for LTP of the RE to CA1 responses, TBS of RE resulted in a significant increase of the RE-evoked SLM sink slope, for the 4 post-TBS periods (LTP1 to LTP4) [$F(4,24) = 6.91$, $P < 0.001$, one-way RM ANOVA], with significant post hoc Newman–Keuls tests shown in Fig. 6a. The RE-evoked SLM sink peak of the group ($n = 7$ mice) was also significantly increased following TBS (data not shown).

The baseline ‘PPF versus $E1$ plot’ could be fitted by a regression line with a negative slope, as shown for an experiment (Fig. 2e). The post-TBS ‘PPF versus $E1$ plot’ showed a less negative slope, and a smaller average PPF, with the average $E1$ shifted to the right (i.e., $E1$ potentiation); all measures at 2–120 min post-TBS were included in the plot (Fig. 2e). For the RE-LTP group, the slope of the PPF versus $E1$ regression line was increased from -1.04 ± 0.19 ($n = 7$) during baseline to -0.80 ± 0.13 ($n = 7$) post-TBS; the increase of the regression line slope was statistically significant [$t(6) = 2.9$, $P = 0.027$, paired t test].

The RE-LTP group showed a decrease in PPF of the RE responses following RE-TBS. Paired-pulses were given at 50 ms IPI in 3 mice, and at 200 ms IPI in 4 mice. Since the baseline PPF did not differ significantly between the 50-ms and 200-ms groups, the two groups were combined.

The combined group ($n = 7$) showed a significant change in PPF with time [$F(4,24) = 6.62$, $P = 0.001$, one-way RM ANOVA], with significant post hoc Newman–Keuls tests shown in Fig. 6a.

In 2 of the 3 mice with DG recording, RE-TBS resulted in potentiation of the RE to DG sink at all post-TBS periods (example shown in Fig. 5). In 4 other mice of the RE-LTP group, the recording probe did not reach the DG. RE to DG excitation was inferred to result from RE activating the EC, which then excited OML and/or MML of the DG (“Discussion”).

TBS of RE did not significantly change the CA1 responses of the non-tetanized stimulus pathway MPP. The example shows a fluctuating time course of the MPP-evoked sink ($E1$) in CA1 SLM, but the sink did not deviate consistently from unity (Fig. 7a). The 30-min averaged CSD profiles show no increase in the sink amplitude at SLM (ch8 and 9) post-TBS (Fig. 7b). However, an increase in an MPP-evoked dipole in the DG (sinks at ch10 and 11, sources at ch13 and 14) was observed post-TBS (Fig. 7a, b). The time course data for the MPP-evoked $E1$ slope, running average of $E1$ (slope) and $E1$ peak at SLM did not show a significant deviation from baseline (Fig. 7c). However, the MPP-evoked $E1$ peak at DG appeared to be potentiated, starting at ~45 min post-TBS (Fig. 7c).

In the RE-LTP group ($n = 7$), 5 mice had an MPP to CA1 response. There was no statistically significant change in MPP-evoked $E1$ in SLM ($n = 5$ mice) during the five time periods after RE-TBS (baseline, LTP1–4), as indicated by a non-significant group effect [$F(4,16) = 0.93$, $P = 0.47$, one-way RM ANOVA; Fig. 6b]. There was also no significant

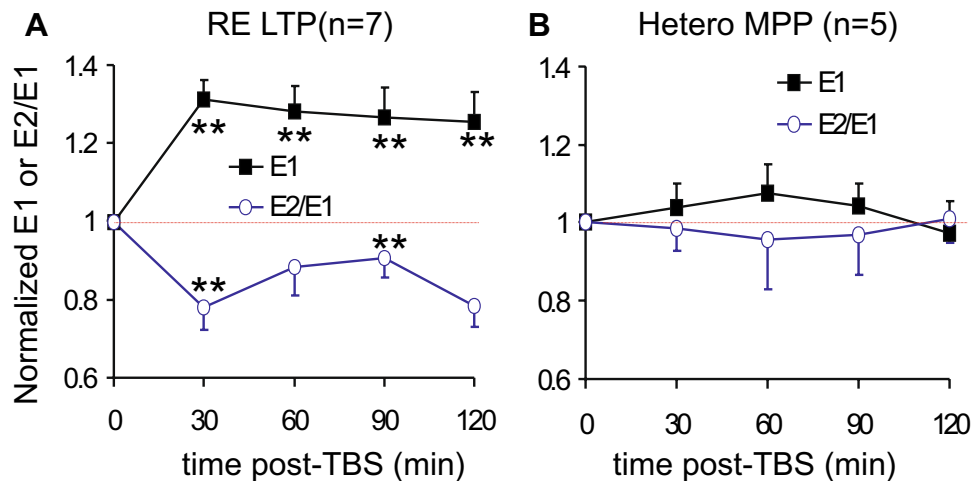
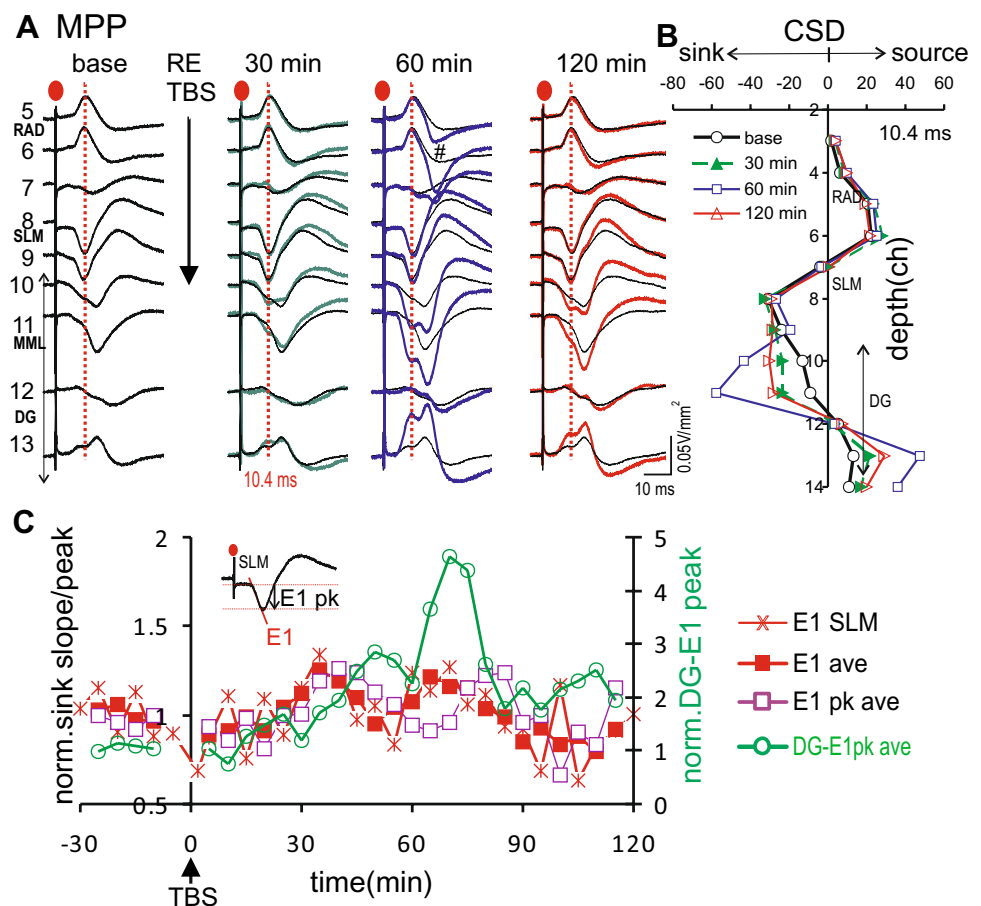


Fig. 6 Group average of RE-evoked and MPP-evoked excitatory sink slope ($E1$) and $E2/E1$ slope ratio in SLM following theta burst stimulation (TBS) of RE, averaged for 30 min intervals. **a** RE response averaged for 30-min blocks: 0 min (–30 to –5 min baseline), 30 min (5–30 min), 60 min (35–60 min), 90 min (65–90 min) and 120 min (95–120 min). $E1$ responses were normalized to baseline, and $E1$

increase post-TBS was generally accompanied by $E2/E1$ decrease. **b**. $E1$ and $E2/E1$ responses to MPP stimulation for the same time periods, available for 5 of 7 mice given RE-TBS, show little change from baseline. ** $P < 0.01$, post hoc Newman–Keuls test after a significant one-way RM ANOVA

Fig. 7 Responses to the non-tetanzed pathway MPP, in experiment of TBS of the RE pathway, same experiment as Fig. 4, with the same layout. **a** Selected channels shown for CA1 responses to MPP stimulus pulses of 60 μ A, during baseline and at 30, 60, 120 min following RE-TBS. Vertical dotted line indicates time of peak MPP-SLM sink at 10.4 ms latency following MPP stimulation. At 60 min, a trisynaptic CA1 response, RAD-sink (#) accompanied by SLM- source appeared together with large MML sinks. **b** MPP evoked average CSD profiles in 30-min time blocks, at 10.4 ms latency. There was little potentiation of the MPP-evoked CSDs in CA1, but potentiation in the DG, maximal sinks at MML, was observed. **c** Time course of *E1* slope and *E1* peak measures of the MPP to CA1 SLM sink, and *E1* peak measure of the MPP to DG MML sink



change in the *E2/E1* ratio of the MPP responses across the five time periods [$F(4,16)=0.11$, $P=0.98$, one-way RM ANOVA; Fig. 6b]. The lack of a significant change of the response to a non-tetanzed pathway means that the LTP of RE-CA1 synapse was input-specific. Of the 7 mice in the RE-LTP group, only 2 had MPP to DG recording, and both mice showed late potentiation of the MPP-evoked DG MML sink, at > 30 min post-RE TBS. The example in Fig. 7 showed large MPP to MML sinks at 60–120 min post-TBS, accompanied by a presumably trisynaptic sink in CA1 RAD at 60 min (# in Fig. 7a).

In summary, the RE to SLM synapse was potentiated after tetanic stimulation (TBS) of RE. LTP of the RE to CA1 synapse was shown by slope and peak measures of the SLM sink, and confirmed by 30-min averages of the CSD depth profile; LTP was accompanied by decrease of PPF. No LTP occurred at the MPP to CA1 synapse. LTP of a presumed polysynaptic RE to DG excitatory sink was also observed.

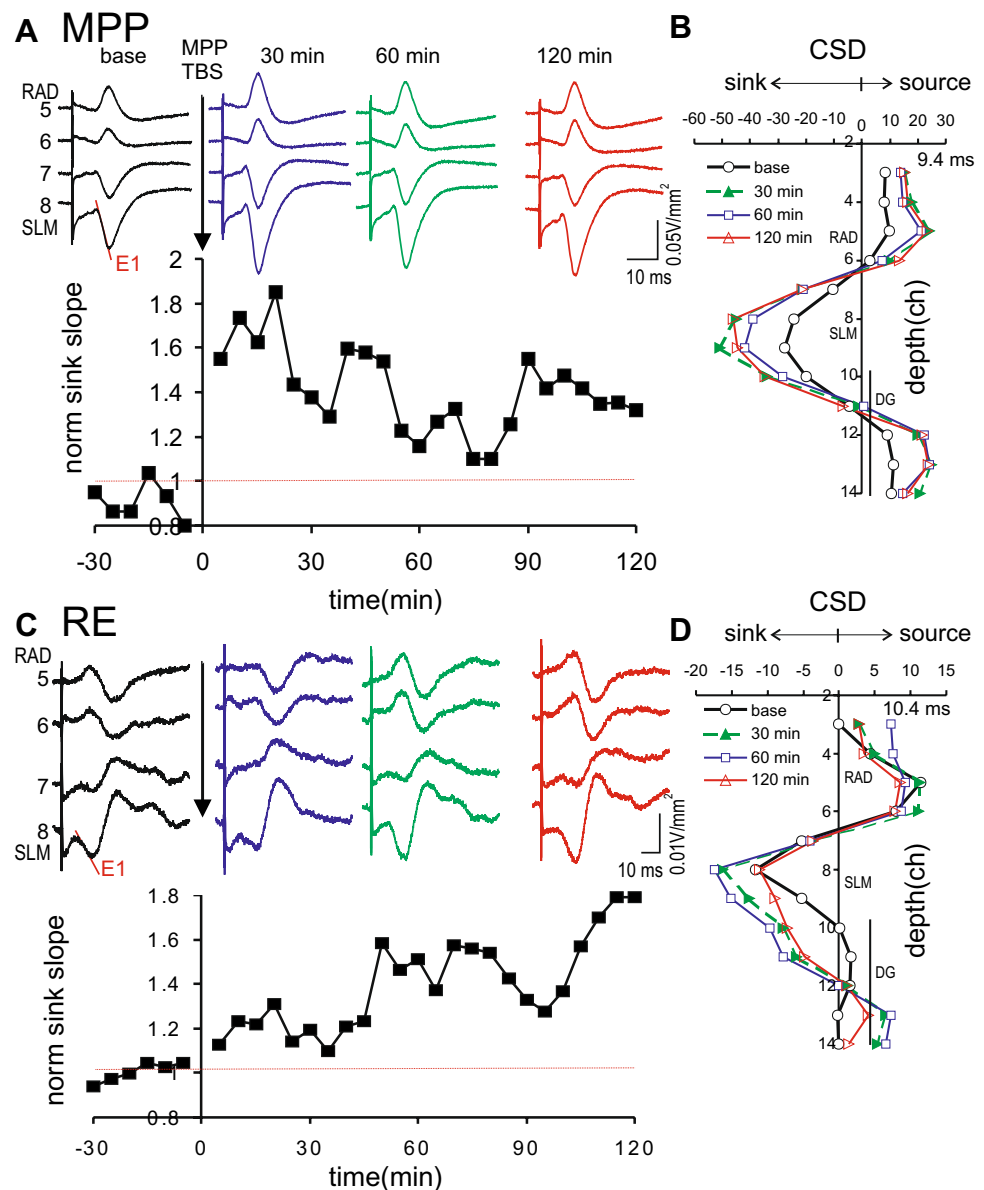
Distal dendritic LTP induced by TBS of MPP

Three groups of mice that were tested for LTP/LTD were categorized. In the MPP-LTP group ($n=7$), TBS of the MPP resulted in LTP in CA1, while no LTP was observed in a

TBS-LTD group ($n=6$). Mice that did not show a large SLM excitation in CA1 ($n=4$), as indicated by presence of RAD-SLM source-sink dipole, as well as mice that did not use the same TBS-recording protocol were excluded ($n=4$). For the MPP-LTP group, test pulses were delivered at $57.1 \pm 10.2 \mu$ A ($n=7$; $2 \times T$ intensity), and TBS pulse intensity was $74.3 \pm 8.4 \mu$ A ($n=7$; $\sim 3.3 \times T$ intensity). The MPP-evoked dipole in CA1, showing a SLM sink and a RAD source, was potentiated after MPP-TBS (Fig. 8a). In the example shown, there was $\sim 60\%$ enhancement of the SLM sink slope immediately post-TBS, followed by a slow temporal decline (Fig. 8a). The CSD profiles, averaged for 30 min periods, showed a clear increase in the CA1 dipole (Fig. 8b) at all post-TBS times compared to baseline; the CA1 dipole consisted of a SLM sink (ch 7–8), and a RAD source (ch 3–6 in Fig. 8a). There was also an increase in a dipole in DG, shown as sinks (ch 9–10) in the molecular layer accompanied by a ventral source (ch 12–14 in Fig. 8b).

Interestingly, the non-tetanzed pathway of RE to SLM excitatory sink showed a slowly increasing potentiation after MPP-TBS (Fig. 8c). At SLM, RE evoked a sink followed by a large source, with each event accompanied by CSD of an opposite polarity at RAD (traces in Fig. 8c). MPP-TBS resulted in enhancement of the RE-evoked temporal CSD

Fig. 8 Long-term potentiation of the MPP- and RE-evoked responses in CA1, shown in a representative mouse, after TBS of the MPP. **a** Average CSD responses ($n=24$ sweeps) following MPP stimuli ($40\ \mu\text{A}$), at selected channels averaged for a 30-min period of baseline (base, -30 min to -5 min), 5 – 30 min (labeled as 30 min), 30 – 60 min (labeled as 60 min), and 90 – 120 min (labeled at 120 min). TBS was delivered to MPP at time 0, and responses were recorded following MPP paired-pulse stimulation; only 1st pulse responses are shown in traces. LTP was observed from the time course of the normalized (norm.) sink slope of the 1st pulse evoked sink ($E1$) at ch 8 (sink spatial maximum), after a 3-point running average. **b** CSD depth profiles at a fixed time instant (9.4 ms latency after MPP stimulation) at the rising phase of the distal dendritic sink (ch8), averaged for 4 periods of time (baseline, 30, 60 and 120 min). **c** Same format as **a** for RE stimulus pulses of $400\ \mu\text{A}$ in the same experiment; RE was not tetanized but RE-evoked sink was enhanced. **d** Same as **b** except for RE evoked average CSD profiles at a fixed time of 10.4 ms latency after RE stimulation



traces at SLM (Fig. 8c). The CSD depth profiles (Fig. 8d) illustrate post-TBS enhancement of the RE-evoked dipole in CA1 (SLM sinks at ch 8 and 9, and RAD sources at ch 4–6). In addition, a RE-evoked DG dipole (sinks at ch 9–10, and sources at ch 13–14; Fig. 8d) appeared to emerge only after MPP-TBS (Fig. 8d).

As expected, the MPP-LTP group showed an increase in MPP-evoked $E1$ slope at SLM across 5 time periods (baseline, LTP1–4), as indicated by a significant group effect [$F(4,24)=6.17$, $P=0.0015$, one-way RM ANOVA; significant post hoc Newman–Keuls tests are indicated in Fig. 9a1]. Paired-pulses were given at 50 ms IPI in 4 mice, and at 200 ms IPI in 2 mice (one mouse with very small PPF was excluded). Since the baseline PPF was not different between the 50-ms and 200-ms groups, the two

groups were combined. The combined group showed a significant decrease in PPF ($E2/E1$) with time [$F(4,20)=6.17$, $P=0.0015$, one-way RM ANOVA, $n=6$], and post hoc Newman–Keuls tests indicated a significant decrease in PPF at 30 and 60 min after TBS compared to baseline (Fig. 9a1). In 4 (of 7) mice of the MPP-LTP group with DG recordings, potentiation of the DG MML sink was seen following MPP-TBS (data included in a group shown in Fig. 9d1).

Two of 7 mice in the MPP-LTP group had RAD to CA1 as a non-tetanized pathway; the RAD to proximal apical dendritic sink in CA1 did not show a consistent change after MPP-TBS. A SLM sink evoked by RE (non-tetanized pathway) was recorded in 3 of 7 mice in the MPP-LTP group (Fig. 9a2). All 3 mice with a RE to SLM sink (Fig. 9a2) showed potentiation of the RE- $E1$ slope or peak.

However, the $n=3$ group did not reveal a statistically significant effect [group effect $F(4,8)=1.40$, $P=0.34$, one-way RM ANOVA]. $E2/E1$ ratio (all at 200 ms IPI) also did not change significantly with the 5 time periods [$F(4,8)=0.96$, $P=0.48$, one-way RM ANOVA]. A DG sink evoked by RE was observed in 2 mice of the MPP-LTP group, of which 1 of the 2 mice showed potentiation of the RE-DG sink after MPP-TBS.

In summary, LTP of the MPP-CA1 synapse was shown by slope and peak measures of the early SLM sink, and by CSD depth profiles; LTP was accompanied by a decrease in PPR. MPP to DG sink and heterosynaptic LTP of the RE-CA1 synapse were observed.

Distal dendritic LTD induced by TBS of MPP

In the MPP-LTD group ($n=6$ mice), MPP-TBS induced LTD of the CA1 SLM sink. The MPP test pulse intensity ($61.7 \pm 12.8 \mu\text{A}$) and TBS intensity ($108.3 \pm 28.8 \mu\text{A}$) were non-significantly ($P > 0.05$, unpaired Wilcoxon) higher than the respective measure in the MPP-LTP group. In a representative mouse of this group, the MPP-evoked SLM sink did not change, while the MPP-evoked MML sink in DG increased nearly two-fold after MPP-TBS (Figs. 8b, 10a1). MPP-TBS also potentiated an MPP-evoked polysynaptic response in CA1 (# in Fig. 10a1). The polysynaptic response was characterized by a RAD sink with sources in PYR and SLM, which corresponded to trisynaptic MPP-DG-CA3-CA1 and disynaptic MPP-CA3-CA1 activation. In the same mouse, the 1st pulse heterosynaptic RE-evoked SLM sink (slope or peak) was higher post-TBS as compared to baseline (Figs. 9a2, 10c), although the 2nd pulse response ($E2$ in Fig. 10a2) was smaller post-TBS compared to baseline.

The MPP-LTD group ($n=6$ mice) showed a significant decrease in the MPP-evoked $E1$ slope in SLM post-TBS [$F(4,20)=6.77$, $P=0.0013$, one-way RM ANOVA; Fig. 9b1]. Paired-pulse ratio $E2/E1$ of the MPP to SLM response was not significantly changed during the post-TBS time periods [$F(4,16)=1.55$, $P=0.24$, one-way RM ANOVA, $n=5$; $E2$ was not available in 1 mouse; Fig. 9b1]. Also, the group ($n=6$) showed a small, non-significant post-TBS increase in the heterosynaptic RE-evoked $E1$ slope in SLM [$F(4,20)=1.58$, $P=0.22$, one-way RM ANOVA; Fig. 9b2], with non-significant change in the RE-evoked $E2/E1$ ratio [$F(4,20)=1.42$, $P=0.26$, one-way RM ANOVA; Fig. 9b2].

Heterosynaptic RE-CA1 response was recorded from 9 mice following TBS of the MPP, combining 3 from the MPP-LTP group and 6 from the MPP-LTD group. As expected, the heterosynaptic RE group ($n=9$) showed no significant change in MPP-evoked SLM sink slope [$F(4,32)=1.80$, $P=0.15$] or $E2/E1$ ratio with time [$F(4,24)=1.02$, $P=0.42$, one-way RM ANOVA; Fig. 9c1]. However, the heterosynaptic RE response

showed a significant increase of the RE-evoked $E1$ sink slope post-TBS [$F(4,32)=2.99$, $P=0.033$, one-way RM ANOVA, $n=9$ mice], giving significant post hoc Newman–Keuls differences at 90 and 120 min post-TBS (Fig. 9c2). There was no significant change in the RE-evoked $E2/E1$ ratio post-TBS [$F(4,32)=1.78$, $P=0.16$, one-way RM ANOVA]. Alternative assessment of potentiation using the RE to SLM $E1$ peak amplitude also showed a statistically significant time effect, using all 5 time periods [$F(4,32)=4.58$, $P < 0.005$, one-way RM ANOVA; inset Fig. 9c2].

Seven mice with DG recording were given an MPP-TBS (including mice in both MPP-LTP and MPP-LTD groups). This group showed a significant increase of the DG-MML sink after MPP-TBS [$F(4,24)=3.76$, $P=0.017$, $n=7$ mice; Fig. 9d1]. Five of the 7 mice had a RE to DG sink, which did not show a significant increase in LTP [$F(4,16)=1.29$, $P=0.32$, Fig. 9d2].

In summary, in a different group of mice, TBS of the MPP resulted in LTD of the MPP-CA1 synapse without significant change in PPR. Irrespective of LTP/LTD at the MPP-CA1 synapse, TBS of the MPP was shown to induce LTP of the RE-CA1 and MPP-DG synapses.

Theta burst stimulation induced sinks in SLM

CSDs during TBS were analyzed in order to elucidate the conditions for LTP or LTD. During the 1st burst (of 10 bursts) of RE-TBS, the SLM sink peaked after the 3rd or 4th pulse within a 10-pulse burst in an example (Fig. 10a). In the RE-LTP group, the average peak latency of the SLM sink was 43.5 ± 4.6 ms from the 1st pulse of the burst ($n=7$ mice, average of 10 sweeps per mouse). The duration of the initial SLM sink of the 1st burst measured 56.9 ± 4.7 ms ($n=7$); the SLM sink of each burst was accompanied by a source of similar duration at RAD (Fig. 10a). The SLM sink amplitude decreased with subsequent bursts (Fig. 10d, average of 10 sweeps). Occasionally, the early RE bursts also induced large sinks at the DG molecular layer, while the example only shows small sinks in DG (inset of Fig. 10a).

For the MPP-LTP group, MPP-TBS evoked large but relatively short-duration initial sinks at SLM during the burst, as shown for a representative mouse (Fig. 10b). Peak SLM sink was evoked by the 1st or 2nd pulse of a 10-pulse burst. The peak latency of the SLM sink was $16.8 \text{ ms} \pm 1.2$ ms from the 1st stimulus pulse ($n=7$ mice, average of 10 sweep per mouse). The duration of the initial SLM sink for the 1st burst measured 32.8 ± 9.3 ms ($n=7$), and the short-duration sink was followed by a prolonged source (see inset in Fig. 10b). The SLM sink peaked with the first few bursts, and ultimately decreased gradually with late bursts (Fig. 10b, d). In addition to sinks at SLM, TBS of the MPP typically induced sinks at the DG molecular layer (ch 10 in Fig. 10b).

SLM sinks evoked by burst stimulation were of higher amplitude, but short duration, for MPP-LTP compared with RE-LTP group. The peak latency of the SLM sink induced by the MPP 1st burst was shorter than that induced by a RE 1st burst (mean 16.8 ms vs 43.5 ms, respectively; $t(12) = 5.63$, $P = 0.0001$, unpaired t test). The duration of the initial sink induced by a MPP 1st burst was also shorter than that induced by RE 1st burst [mean 32.8 ms vs 56.9 ms, respectively; $t(12) = 2.32$, $P = 0.04$, unpaired t test].

For the MPP-LTD group, CSDs during TBS for a representative mouse showed small SLM (ch 9) and large DG (ch 11) sinks during the bursts (Fig. 10c). All mice in the MPP-LTD group showed a large MML to SLM sink ratio (sum of sinks activated in DG/sum of sinks activated in SLM) induced by the 1st burst, measuring 3.22 ± 0.9 ($n = 5$ mice). By comparison, the 1st burst gave low MML to SLM sink ratio in 4 of 5 mice in the MPP-LTP group with DG recording, with a ratio of 0.71 ± 0.27 ($n = 4$; one outlier had a ratio of 8.1). The peak latency of the burst-activated SLM sink (averaged from 100 bursts) measured 33.6 ± 3.8 ms ($n = 6$) in the MPP-LTD group, significantly ($P < 0.003$, unpaired Wilcoxon) later than 16.8 ± 1.2 ms ($n = 7$) in the MPP-LTP group. By contrast, the peak latency of the DG sink was not significantly different between MPP-LTP and MPP-LTD groups, measuring (in mice with DG recordings) 21.1 ± 2.2 ms ($n = 5$) and 18.7 ± 2.8 ms ($n = 5$), respectively. Thus, LTD of the MPP to SLM synapse may result when the DG (relative to SLM) received strong activation from MPP stimulation, and strong DG activation may provide strong inhibition to suppress LTP at the SLM of CA1 (see “Discussion”). However, peak amplitude, total area, or duration of CA1 SLM sink did not differ significantly ($P > 0.05$) between the MPP-LTP and MPP-LTD groups.

Post hoc analysis of the histological section with the MPP electrode indicated that the electrode was preferentially placed in a medial position of the angular bundle (Fig. 1a) in the MPP-LTP group, as compared to a more lateral position in the MPP-LTD group (not shown). Semi-quantitative assessment of the MPP electrode position (assigning medial, intermediate and lateral placements as 1, 1.5 and 2, respectively) gave a mean of 1.29 ($n = 7$) and 1.75 ($n = 6$) for the MPP-LTP and MPP-LTD groups, respectively, with a marginally non-significant difference between the groups ($P = 0.095$, unpaired Wilcoxon).

A progressive and robust increase in the polysynaptic RAD sink (# in Fig. 10d) was found in some mice during the late bursts of MPP-TBS. The burst-activated RAD sinks predicted the LTP of the MPP to polysynaptic CA1 sink in RAD (# in Fig. 10a1, same mouse as in Fig. 10c). Including both MPP-LTP and MPP-LTD groups, 6 of 7 mice with large and increasing RAD sinks during TBS showed potentiation of the MPP-CA1 polysynaptic sink in RAD, while all 6 mice that did not show large RAD sinks during TBS also did not

show potentiation of the MPP-CA1 polysynaptic sink. MPP to CA1 responses was monitored at $2 \times T$ stimulus intensity. The accuracy of predicting LTP of the MPP to CA1 polysynaptic (RAD) sink was thus 12/13 (92.3%).

In summary, the CSDs during TBS showed declining excitatory SLM sinks in response to repeated burst stimulation, with briefer but larger burst-induced sinks for MPP than RE. The MPP-LTP group showed high SLM sinks and relatively low DG sinks during TBS, while MPP-LTD group showed the reverse. Repeated, sharp RAD sinks during TBS predicted accurately the occurrence of LTP at the polysynaptic MPP to CA1 sink.

Discussion

Physiology of the RE-CA1 distal dendritic synapses

RE stimulation in mice activated a CA1 SLM sink at ~ 9 ms onset latency, interpreted to be a monosynaptic excitation of distal apical dendrites of CA1 pyramidal cells (Herkenham 1978; Wouterlood et al. 1990). The excitatory current sink at the distal apical dendrites of CA1 pyramidal cells (SLM) was accompanied by a current source at the proximal apical dendrites (RAD). The profile of CSD in the hippocampus after RE stimulation in mice was similar to that reported in rats (Dolleman-Van der Weel et al. 1997; Hauer et al. 2019). We also confirmed that RE stimulation did not evoke a population spike in the hippocampus (Dolleman-Van der Weel et al. 1997; Hauer et al. 2019; however, see Bertram and Zhang 1999), even at high stimulus intensity (600 μ A).

The average RE stimulus threshold intensity (~ 300 μ A) to activate a CA1 response, compared to the MPP (~ 30 μ A) indicates a large chronaxie (an excitability time parameter) for activating action potentials from cell bodies in RE compared to myelinated axons in MPP (Nowak and Bullier 1998). Higher extracellular stimulation currents are needed to activate soma than axon because the extracellular somatic currents need to spread and initiate an action potential from an electronically remote site, the axon initial segment (Rattay et al. 2012).

At long latencies (150–200 ms) after RE stimulation, a dipole of SLM-source and RAD-sink was observed, opposite in polarity to the initial dipole of SLM-sink and RAD-source. The late SLM source is suggested to result from late (> 100 ms latency) inhibition of the distal apical dendrites, likely contributed by GABA_B receptor activation by neurogliaform cells (Price et al. 2008; Capogna 2011). An early GABA_A receptor-mediated inhibition of the distal apical dendrites at ~ 30 ms latency may also be suggested. Some GABAergic interneurons in RAD, called PP-associated interneurons, have specific axonal projection to the distal apical dendrites (Hajos and Mody 1997; Klausberger

2009); a specific group was shown to mediate GABA_A receptor-mediated inhibition (Lasztozci and Klausberger 2014). GABAergic interneurons in stratum oriens (O-LM interneurons) also project specifically to SLM but whether they are activated by RE or MPP stimulation is not known. GABAergic interneurons in CA1 were known to be innervated by RE afferents (Dollerman-Van der Weel and Witter 2002; Wouterlood et al. 1990) and putatively activated by RE stimulation (Dolleman-Van der Weel et al. 1997).

RE stimulation was shown to activate the DG molecular layer weakly during baseline, at a small but significant delay (~2.7 ms) from the onset of the CA1 (SLM) sink. We infer that RE excitation of the DG was at least disynaptic, possibly following a sequence of RE-EC-DG. A direct RE projection to the DG was not revealed by neuroanatomical studies (Herkenham 1978; Wouterlood et al. 1990). Thus, we suggest that RE first activated the lateral and medial EC (Herkenham 1978; Yanagihara et al. 1987; Wouterlood et al. 1990; Wouterlood 1991), which then excited DG. Instead of traversing the cingulum like RE to CA1 afferents (Wouterlood et al. 1990), RE afferents to EC may travel through a shorter (and faster) ventral thalamo-temporal pathway. RE had to fire EC neurons shortly before the RE-SLM sink onset, in order to generate a DG molecular layer sink at ~3 ms after RE-SLM sink onset. OML and MML excitatory sinks likely resulted from activating layer II neurons in lateral and medial EC, respectively.

Identification of MPP-CA1 distal dendritic excitatory sink

MPP stimulation in mice activated a distal apical dendritic (SLM) sink in CA1, accompanied by a source in RAD; the CA1 dipole was almost identical to that following RE stimulation. MPP stimulation consistently activated a molecular layer sink in DG, with a source near the granule cell layer (Figs. 4b, 7b, 11a). The voltage and CSD profiles in mice were similar to those reported following MPP/EC stimulation in rats (Leung et al. 1995; Leung and Peloquin 2010; Dolleman-Van der Weel et al. 2018) and rabbits (Yeckel and Berger 1990).

Gamma oscillations in hippocampal CA1

In about half of the mice, single-pulse stimulation of RE activated more than one SLM sink peak, with peaks occurring at 20–40 ms interpeak intervals, i.e., at a gamma frequency of 25–50 Hz. Similar oscillatory responses in CA1 were not observed after MPP stimulation, perhaps because they were suppressed by prolonged feed-forward inhibition after MPP activation of the DG and CA3. In addition, spontaneous gamma LFPs revealed CSDs that resemble the SLM-RAD dipole evoked by RE (or MPP) stimulation, with

an abrupt phase reversal at the RAD-SLM border. Gamma oscillations with a SLM-RAD dipole have been shown in previous studies (Charpak et al. 1995; Benito et al. 2014; Lasztozci and Klausberger 2014, 2017).

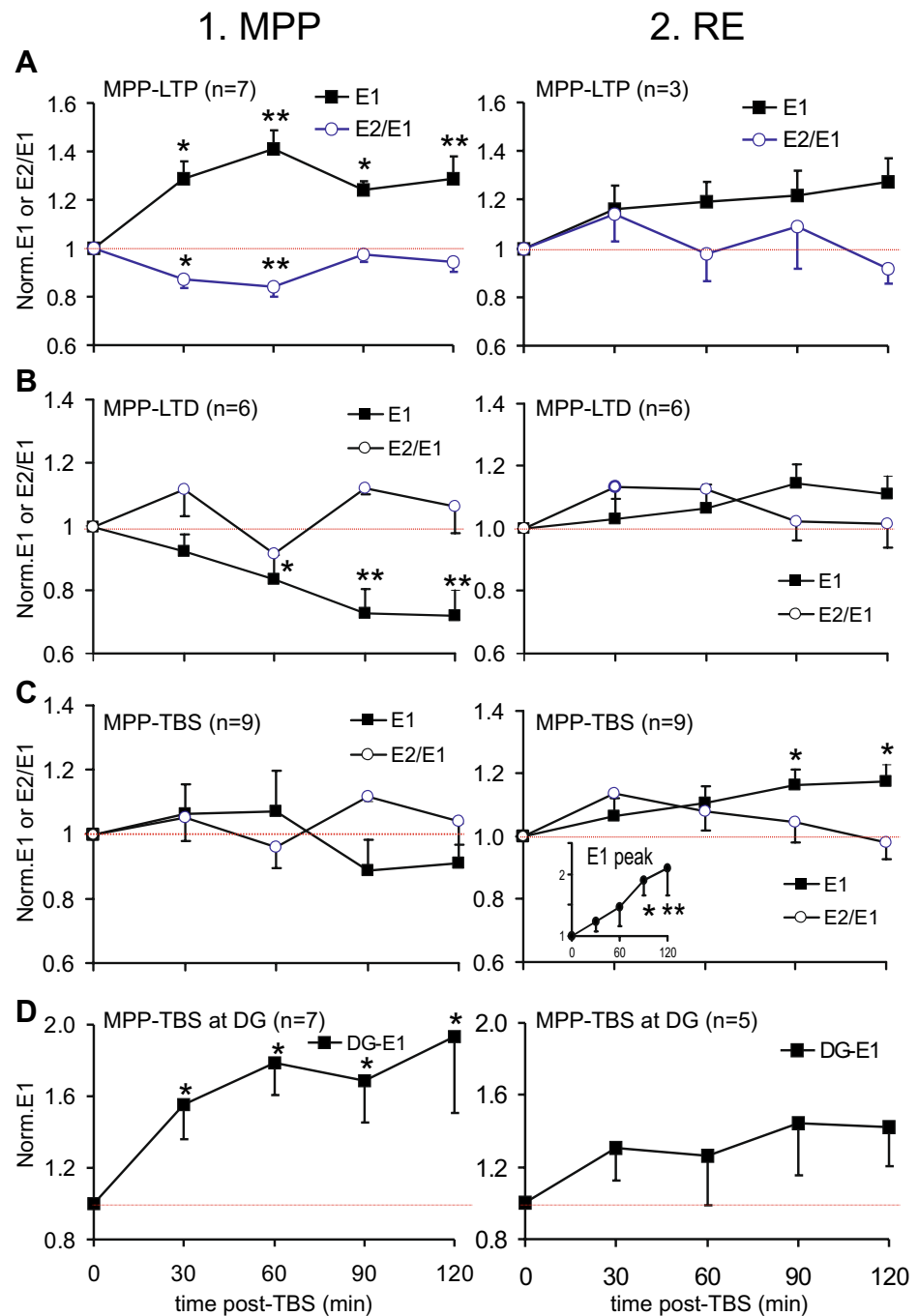
Gamma oscillations may have an extrinsic or intrinsic origin. Afferents from EC layer 3 pyramidal cells were suggested to drive a distal dendritic gamma in CA1, in the 30–60 Hz frequency range in isolated guinea pig brains (Charpak et al. 1995) or urethane-anesthetized rats (Bragin et al. 1995; Lasztozci and Klausberger 2014, 2017). EC driven gamma in SLM was in the 60–140 Hz frequency range in behaving animals (Belluscio et al. 2012; Colgin et al. 2009; Chrobak and Buzsáki 1998; Fernandez-Ruiz et al. 2017). Intrinsic networks of inhibitory interneurons (Jefferys et al. 1996) or excitatory and inhibitory neurons (Leung 1982; Csicsvari et al. 2003; Mann et al. 2005) could generate distal-dendritic gamma oscillations, but the participating neurons have not been identified, except for RAD interneurons that provide GABA_A receptor-mediated inhibition to SLM (Lasztozci and Klausberger 2014). RE afferents to CA1 may also drive or modulate SLM gamma activity, but direct evidence is so far lacking, and unitary recordings did not identify gamma activity in the RE (Morales et al. 2007; Hauer et al. 2019). Regardless of generating mechanism, the prominent distal dendritic gamma oscillations in CA1 may play a role in processing RE neural signals, in support of neural functions such as feature binding, perception, and memory encoding (Kay and Freeman 1998; Fries et al. 2007; Lisman and Jensen 2013).

Paired-pulse facilitation of the distal dendritic synapses

PPF in the 20–200 ms IPI was found more readily after RE than MPP stimulation. PPF is explained by presynaptic facilitation, or an increase release of neurotransmitter by the 2nd pulse as compared to the 1st pulse (Wu and Saggau 1994; Zucker and Regehr 2002). However, postsynaptic factors may also affect PPF, including Ca²⁺-dependent protein kinases (Wang and Kelly 1997) and postsynaptic inhibition (Leung et al. 2008). The decline of PPF with *E1* (Fig. 2e), or with increasing stimulus intensity, may suggest a saturation of either postsynaptic electromotive force or presynaptic release (Leung and Fu 1994). However, a change in PPF-*E1* relation post-TBS may involve a presynaptic mechanism, and a stronger presynaptic release is associated with lower PPF. The average PPF (*E2/E1*) of distal dendritic synapses was decreased after LTP induction at either RE (Fig. 6a) or MPP afferents (Fig. 9a1). LTP of the Schaffer's collaterals to CA1 synapses could be associated with (Schulz et al. 1994) or without PPF decrease in vitro (Manabe et al. 1993).

A PPR ≈ 1 for MPP stimulation seems to be different from the PPF reported in other studies (Dolleman-van der

Fig. 9 Group average of MPP-evoked and RE-evoked excitatory sink $E1$ and $E2/E1$ ratio in SLM, and MPP evoked dentate gyrus (DG) sink, following theta burst stimulation (TBS) of MPP, averaged for 30 min intervals. **a** MPP-LTP group selected for LTP of the MPP to CA1 SLM responses. Column 1, MPP-evoked responses in SLM: 1st pulse excitatory sink slope $E1$, and $E2/E1$ ratio, averaged for four 30-min time periods ending at 0, 30, 60, 90 and 120 min. Column 2, $E1$ and $E2/E1$ responses in CA1 SLM following RE stimulation (not tetanized) were available for 3 of 7 mice in the MPP-LTP group. $*P < 0.05$, and $**P < 0.01$, post hoc Newman-Keuls test after a significant one-way RM ANOVA apply to the whole figure. **b** MPP-LTD group selected for LTD of the MPP to SLM responses. Column 1, MPP-evoked $E1$ response in SLM showed gradual decrease with time, and no clear change in $E2/E1$. Column 2, RE-evoked $E1$ and $E2/E1$ responses in CA1 SLM. **c** Group of 9 mice given MPP-TBS with RE-evoked responses (including 3 mice shown in A2). Column 1, MPP-evoked SLM sinks showed no significant change of $E1$ or $E2/E1$ with time, while column 2 shows a significant increase in RE-evoked $E1$ (sink slope) and $E1$ peak (inset) in late time periods. **d** Group of MPP-TBS mice ($n = 7$) with DG recording showed significant LTP of the MPP to DG sink (column 1) but no significant change of the RE-DG sink ($n = 5$ mice)



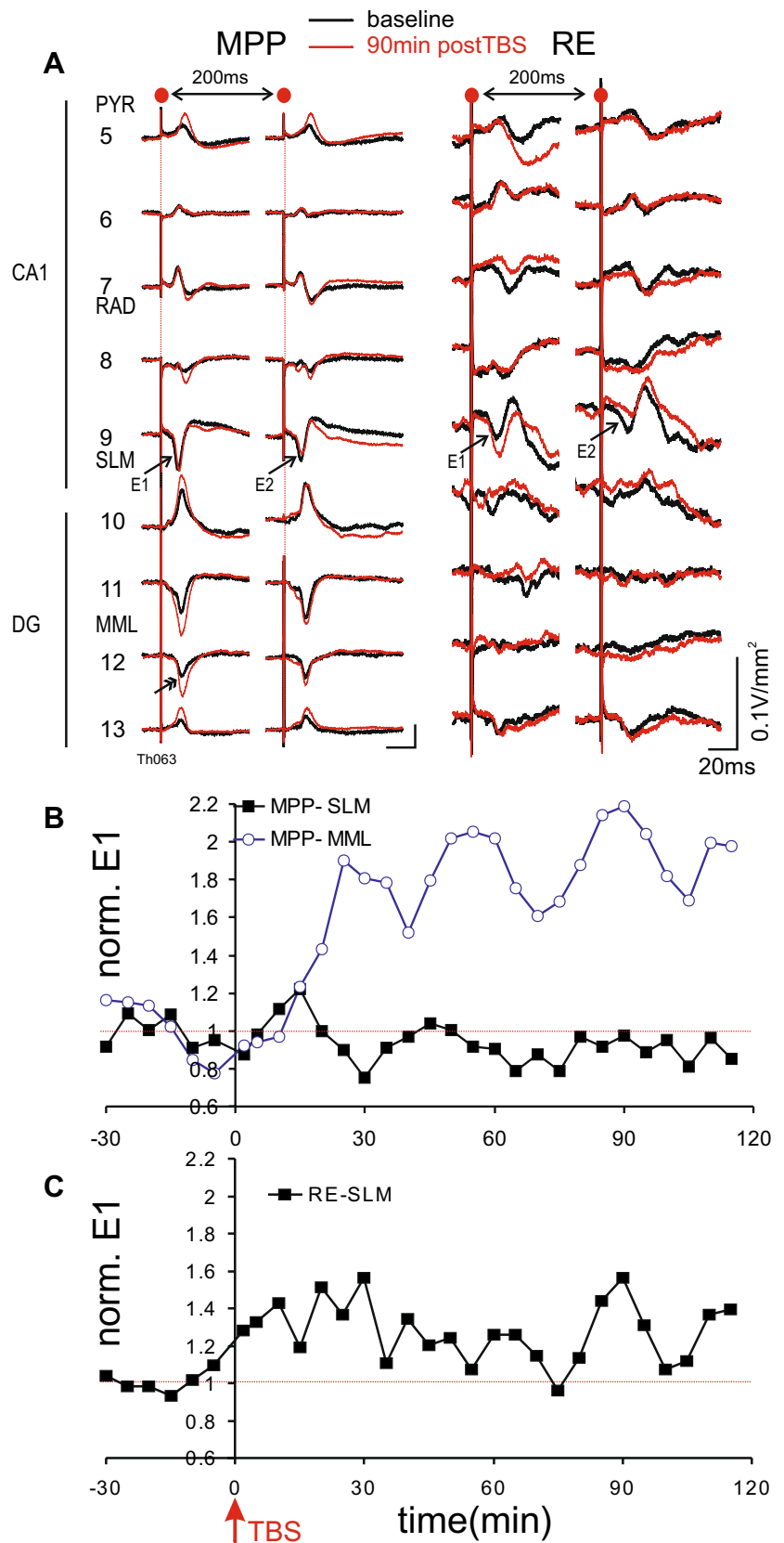
Weel et al. 2017; Gugustea et al. 2019). The reason for this is not clear, but a stronger GABAergic inhibition of SLM by MPP stimulation may be suggested.

Conditions necessary for LTP at the distal apical dendritic synapses

LTP of the SLM sink in CA1 was readily elicited following RE-TBS, despite using low ($\sim 1.7 \times T$) stimulus intensity for TBS. Other than TBS, no other tetanic stimulus patterns

had been systematically studied. During burst stimulation, the slow rise of the RE to SLM current sink in ~ 30 ms, and sink duration of ~ 45 ms, may suggest activation of an NMDA receptor-mediated current. The gradual rise of the sink within a burst may result from paired- or multiple-pulse facilitation during TBS (Creager et al. 1980). However, repeated bursts at 200 ms intervals (5-Hz frequency) only evoked decremental SLM sink responses (Fig. 10a, c). Also, the next sweep of 10 bursts, delivered 10 s later, did not evoke a higher SLM response (data not shown). These

Fig. 10 Heterosynaptic potentiation of RE-evoked CA1 sink was found in mouse without potentiation of the MPP-evoked CA1 sink. **a** Column 1, average CSDs ($n=20$ sweeps), following MPP paired-stimulation at 200 ms IPI, during baseline and at 90–110 min after TBS of the MPP. Initial $E1$ dipole in CA1 (SLM sink and RAD source) was unchanged after MPP TBS, while dipole in dentate gyrus (DG), with double-headed arrow pointing at middle molecular layer (MML) sink at channel 12, was potentiated. Column 2, average CSDs ($n=24$ sweeps) following paired-pulse stimulation (200 ms IPI) of RE show enhancement of 1st pulse responses ($E1$ at SLM). **b** MPP-evoked responses (3-point running average) shows a post-TBS increase in normalized $E1$ at MML but not at SLM. **c** RE-evoked $E1$ sink at SLM (3-point running average) shows a small but consistent potentiation post-TBS



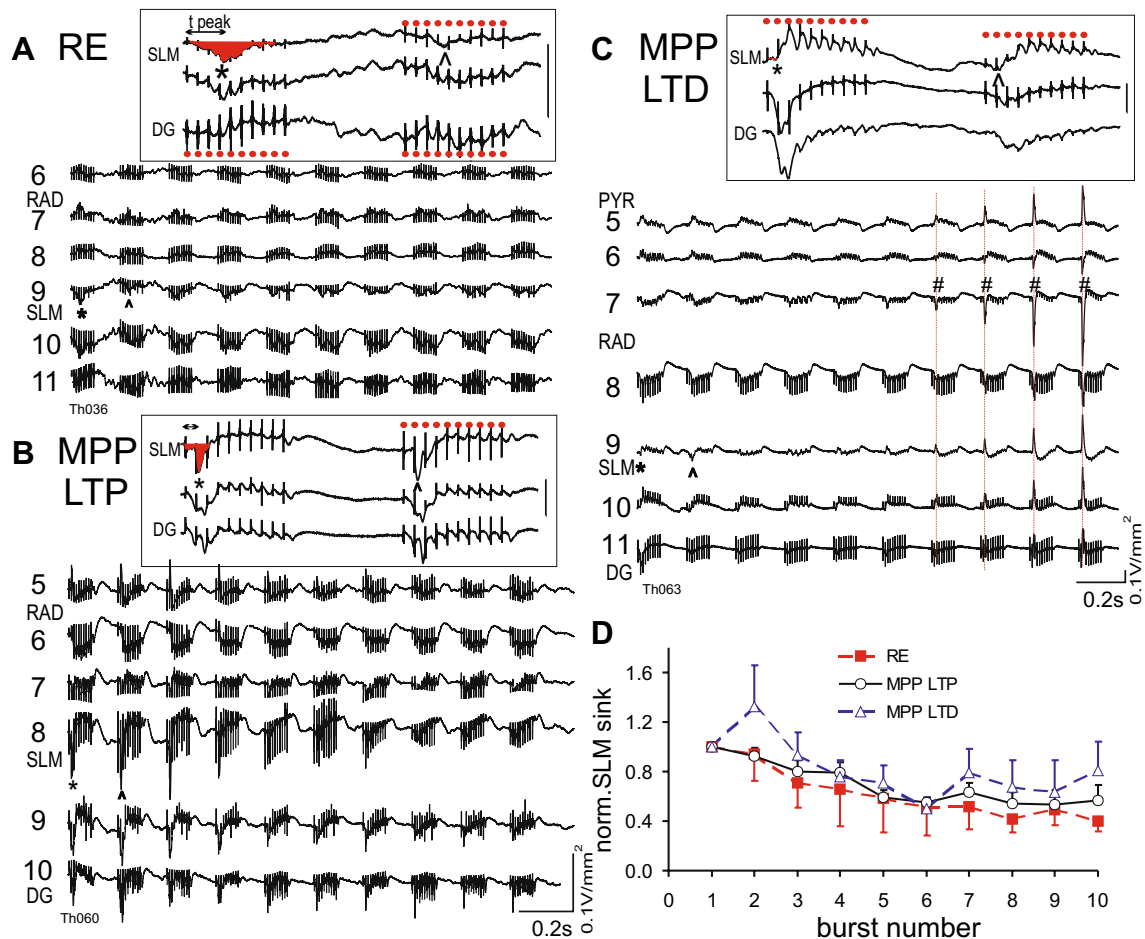


Fig. 11 CSDs evoked during theta-burst stimulation (TBS) of RE and MPP. **a** CSDs during burst stimulation of the RE (average of 10 sweeps; each sweep had 10 bursts, with 10 pulses at 100 Hz per burst) induced a slowly rising excitatory sink at the distal apical dendrites (SLM), but generally decremental responses with subsequent bursts. Stimulus artifacts (vertical lines) were truncated. Inset at top is a magnified view of the first 2 bursts at SLM and adjacent dentate gyrus (DG). Asterisk, peak sink for 1st burst indicated by time 't peak'; sink area colored in red; circumflex accent, peak sink for 2nd burst; stimulus artifacts labeled by red dots; calibration 0.1 mV/mm². **b** Representative example of burst stimulation of MPP that

induced LTP of the SLM sink. A burst typically evoked large but relatively brief SLM sink (inset), with peak SLM sinks also decreasing with subsequent bursts. **c** Representative example of MPP-TBS that induced LTD of the MPP-evoked SLM sink. SLM sink was less apparent during the initial bursts (inset). In this example, polysynaptic CA1 sinks (vertical lines labeled by #) at RAD, accompanied by sources at PYR and SLM, gradually increased with late bursts. **d** Group average of burst-induced peak SLM sinks show similar decline with repeated bursts given to either RE or MPP, irrespective of whether MPP induced LTP or LTD. The SLM sinks were normalized by the peak sink evoked by the 1st burst

characteristics suggest that a single burst (delivery of 10 pulses at 100 Hz), but not repeated theta-frequency bursting, was critical to potentiate the SLM sink. However, measures of SLM sink magnitude/duration did not correlate with the degree of LTP/LTD in RE-TBS or MPP-TBS experiments.

A successful prediction of LTP of the MPP to CA1 polysynaptic sink could be made based on activation of a high-amplitude RAD sink- PYR source dipole (# in Fig. 10d). Theta and 1-Hz frequency bursting is known to enhance Schaffer-collaterals mediated excitation in the hippocampus (Herrerias et al. 1987; Fung et al. 2016; Thomas et al. 1998). Low-frequency stimulation (1–20 Hz) is known to activate the CA3 and CA1 synapses in an EC-hippocampal

multisynaptic circuit, while high-frequency stimulation (100–400 Hz) is optimal to activate the MPP-DG and MPP-CA1 synapses (Yeckel and Berger 1998). These results are consistent with our observation that RE or MPP to SLM responses were optimally facilitated during 100-Hz pulses and not by theta (5-Hz) frequency bursts.

We assessed LTP in CA1 and DG following TBS of MPP. Only about half of mice selected for a clear MPP to CA1 sink in SLM showed LTP of this SLM sink after TBS of the MPP (the MPP-LTP group), while the rest of the mice showed LTD on average (the MPP-LTD group). Recording of CSDs during TBS showed that the MPP-LTP group manifested large SLM (CA1) sink and small MML (DG)

sink, while MPP-LTD group showed large activation of the DG as compared to SLM, with peak activation earlier in the DG than in SLM (Results). The MPP electrode tended to be located more medially (non-significantly) in the angular bundle for the MPP-LTP as compared to the MPP-LTD group. Tetanic stimulation of the MPP electrode could excite EC to CA1 afferents (layer 3 cells from the medial or lateral EC) or EC to DG/CA3 (EC layer 2 cells) and backfiring of MPP to subiculum fibers that could form en passant synapses in CA1 (cf. Witter et al. 1989). A lateral placement in the angular bundle may activate more the afferents of lateral EC that preferentially project to the DG (outer molecular layer) and shift the maximal response location in CA1.

Homosynaptic and heterosynaptic LTP at the distal apical dendrites

Despite the relatively low amplitude of excitatory sink at the distal dendrites, TBS of the RE readily induced 20–30% LTP of RE-SLM sink for at least 2 h. A CA1 dipole, consisting of an excitatory SLM sink and a RAD source, was potentiated (Fig. 5b). LTP of the RE-SLM synapse was input-specific, and there was no LTP of the non-tetanized MPP-SLM synapse in the same group of animals. The LTP was generally accompanied by a decrease in PPF.

In a group selected for MPP-LTP ($n = 7$), MPP-TBS induced 20–30% LTP of the MPP-SLM sink for a duration of 2 h. In a different group showing LTD of the MPP-SLM sink ($n = 6$), 10–20% LTD of the MPP-SLM sink was observed after MPP-TBS. Interestingly, irrespective of LTP or LTD of the MPP-SLM sink, MPP-TBS induced potentiation of the heterosynaptic, RE to SLM sink at 60–120 min after TBS (Fig. 9b2).

Heterosynaptic potentiation of the RE-SLM sink after MPP-TBS may result from different reasons. There could be ephaptic interactions among the synapses and distal dendrites in SLM. For example, RE to SLM synaptic responses may be enhanced by presynaptic facilitation through ephaptic feedback of the MPP-evoked excitatory postsynaptic potential (Kasyanov et al. 2000), or by an ephaptic effect on Ca^{2+} transients in the distal dendritic tufts (Maeda et al. 2015). Dolleman-van der Weel et al. (2017) reported more than linear summation of the SLM sink response when both MPP and RE were stimulated simultaneously. However, the reverse potentiation of MPP-SLM synapses after RE-TBS was not found, which suggests MPP-TBS can increase RE-SLM synaptic transmission, but RE-TBS did not increase MPP-SLM transmission. Lack of MPP-SLM heterosynaptic LTP could be because of the small fraction of RE-SLM afferents that was activated by MPP. Also, there is a more mundane explanation that RE afferents may be activated by MPP stimulation at the angular bundle, and not vice versa. In the rat, Wouterlood (1991) described labeled RE fibers

to “curve ventrally around the splenium to enter the angular bundle” during their course to CA1 and dorsal subiculum. Thus, RE fibers that travel near the angular bundle may be activated by MPP stimulation in the present study. The activated RE fibers would add to the MPP to SLM excitation, and would also be activated during MPP-TBS. If the same RE to SLM fibers were activated by both RE stimulus and MPP-TBS, LTP of the RE to SLM synapses may be expected. In another LTP model in which a weaker pathway (contralateral EC to DG) was tetanized together with a stronger pathway (ipsilateral EC to DG) that induced LTP, associative LTP was observed in the weaker pathway (Levy and Steward 1979). The present study, however, presents a different scenario that the stronger MPP-CA1 pathway manifested LTD, while the weaker RE to CA1 pathway showed LTP. Within the densely packed neuropil in SLM, perhaps depolarization of RE presynaptic terminals by MPP afferent (stronger pathway) activity can happen via ephaptic interaction or extracellular (K^+) ions. Further studies are needed to clarify the mechanism of heterosynaptic RE-SLM LTP, and independent stimulation of RE and MPP fibers (by optogenetic stimulation) may be necessary.

In a small number of experiments that recorded from DG, heterosynaptic LTP of the MPP-DG synapse was observed after RE-TBS, and less frequently, heterosynaptic LTP of the RE-DG synapses was seen after MPP-TBS. A disynaptic, RE to DG excitation through the lateral and medial EC may explain heterosynaptic LTP at the MPP to DG synapses. Similarly, potentiation of a polysynaptic EC to CA1 circuit (i.e., RE-EC-CA1) may account for the large heterosynaptic LTP of the RE to CA1 sink, especially the *E1* peak (Fig. 8c inset). However, polysynaptic potentiation may not adequately explain potentiation of the short-latency sink slope (*E1* slope), and it is paradoxical that polysynaptic LTP of RE-CA1 synapses should occur with LTD of the MPP-CA1 synapses.

Heterosynaptic LTP following repeated activation of the EC to CA1 pathway may have behavioral significance. Assume that EC to CA1 afferents encode the spatial location of an animal, and RE to CA1 afferents represent an affective component of the event such as fear. Heterosynaptic potentiation of RE to CA1 afferents following repeated activity of the EC to CA1 afferents may facilitate the encoding of a place associated with fear, or the perceptual binding of place and fear. In general, heterosynaptic potentiation could serve to induce LTP of a synaptic pathway that only evokes weak postsynaptic response, and Hebbian LTP occurs in association with strong postsynaptic depolarization provided by other inputs. In addition, the spontaneous gamma oscillation at the distal dendrites is a wave of membrane depolarization that would facilitate LTP and encoding at specific phases, as has been shown for the theta rhythm (Law and Leung 2018).

Conclusion

The RE to SLM pathway showed robust PPF and propensity for LTP and evoked gamma oscillations. Short-term and long-term synaptic plasticity are likely important for neural processing and memory encoding, with gamma oscillations possibly playing a role in processing and integration of neural signals from both RE and EC.

Acknowledgements We thank the laboratory of Vania and Marco Prado for the supply of mice, and L. Chiu for technical support.

Funding Funded by operating Grants from the Canadian Natural Sciences and Engineering Research Council (1037-2013) and Canadian Institutes of Health Research (CIHR) MOP-15685 (to LSL).

Compliance with ethical standards

Conflict of interest The authors declare that they have no conflict of interest.

Ethical standards All procedures performed in studies involving animals were in accordance with the ethical standards of the institution or practice at which the studies were conducted. Approved by Western University Animal Care Committee, Animal Use Protocol 2010-261.

References

- Aksoy-Aksel A, Manahan-Vaughan D (2015) Synaptic strength at the temporoammonic input to the hippocampal CA1 region in vivo is regulated by NMDA receptors, metabotropic glutamate receptors and voltage-gated calcium channels. *Neuroscience* 309:191–199
- Al-Onaizi MA, Parfitt GM, Kolisnyk B, Law CSH, Guzman MS, Barros DM, Leung LS, Prado MAM, Prado VF (2016) Regulation of cognitive processing by hippocampal cholinergic tone. *Cereb Cortex*. <https://doi.org/10.1093/cercor/bhv349>
- Amaral DG, Witter MP (1989) The three-dimensional organization of the hippocampal formation: a review of anatomical data. *Neurosci* 31:571–591
- Belluscio MA, Mizuseki K, Schmidt R, Kempter R, Buzsáki G (2012) Cross-frequency phase-phase coupling between θ and γ oscillations in the hippocampus. *J Neurosci* 32:423–435
- Benito N, Fernandez-Ruiz A, Makarov VA, Makarova J, Korovai-chuk A, Herreras O (2014) Spatial modules of coherent activity in pathway-specific LFPs in the hippocampus reflect topology and different modes of presynaptic synchronization. *Cereb Cortex* 24:1738–1752
- Bertram EH, Zhang DX (1999) Thalamic excitation of hippocampal CA1 neurons: a comparison with the effects of CA3 stimulation. *Neuroscience* 92:15–26
- Bliss TVP, Collingridge G, Morris R (2007) Synaptic plasticity in the hippocampus. In: Andersen P, Morris R, Amaral D, Bliss T, O'Keefe J (eds) *The hippocampus book*. Oxford University Press, Oxford, pp 343–434
- Bragin A, Jando G, Nádasdy Z, Hetke J, Wise K, Buzsáki G (1995) Gamma frequency (40–100 Hz) patterns in the hippocampus of the behaving rat. *J Neurosci* 15:47–60
- Brun VH, Leutgeb S, Wu HQ, Schwarcz R, Witter MP, Moser EI, Moser MB (2008) Impaired spatial representation in CA1 after lesion of direct input from entorhinal cortex. *Neuron* 57:290–302
- Brun VH, Otnæss MK, Molden S, Steffenach HA, Witter MP, Moser MB, Moser EI (2002) Place cells and place recognition maintained by direct entorhinal-hippocampal circuitry. *Science* 296:2243–2246
- Capogna M (2011) Neurogliaform cells and other interneurons of stratum lacunosum-moleculare gate entorhinal-hippocampal dialogue. *J Physiol* 589:1875–1883
- Chapak S, Pare D, Llinas R (1995) The entorhinal cortex entrains fast CA1 hippocampal oscillations in the anaesthetized guinea-pig: role of the monosynaptic component of the perforant path. *Eur J Neurosci* 7:1548–1557
- Cholvin T, Loureiro M, Cassel R, Cosquer B, Geiger K, De Sa ND, Raingard H, Robelin L, Kelche C, Pereira de Vasconcelos A, Cassel JC (2013) The ventral midline thalamus contributes to strategy shifting in a memory task requiring both prefrontal cortical and hippocampal functions. *J Neurosci* 33:8772–8783
- Chrobak JJ, Buzsáki G (1998) Gamma oscillations in the entorhinal cortex of the freely behaving rat. *J Neurosci* 18:388–398
- Clement EA, Richard A, Thwaites M, Ailon J, Peters S, Dickson CT (2008) Cyclic and sleep-like spontaneous alternations of brain state under urethane anaesthesia. *PLoS ONE* 3(4):e2004
- Colgin LL, Denninger T, Fyhn M, Hafting T, Bonnevie T, Jensen O, Moser MB, Moser EI (2009) Frequency of gamma oscillations routes flow of information in the hippocampus. *Nature* 462:353–357
- Creager R, Dunwiddie T, Lynch G (1980) Paired-pulse and frequency facilitation in the CA1 region of the in vitro rat hippocampus. *J Physiol (Lond)* 299:409–424
- Csicsvari J, Jamieson B, Wise KD, Buzsáki G (2003) Mechanisms of gamma oscillations in the hippocampus of the behaving rat. *Neuron* 37:311–322
- Davoodi FG, Motamedi F, Naghdi N, Akbari E (2009) Effect of reversible inactivation of the reuniens nucleus on spatial learning and memory in rats using Morris water maze task. *Behav Brain Res* 198:130–135
- Dolleman-van der Weel MJ, Lopes da Silva FH, Witter MP (2017) Interaction of nucleus reuniens and entorhinal cortex projections in hippocampal field CA1 of the rat. *Brain Struct Funct* 222:2421–2438
- Dolleman-van der Weel MJ, Morris RG, Witter MP (2009) Neurotoxic lesions of the thalamic reuniens or mediodorsal nucleus in rats affect non-mnemonic aspects of watermaze learning. *Brain Struct Funct* 213:329–342
- Dolleman-van der Weel MJ, Witter MP (2000) Nucleus reuniens thalamic innervates gamma aminobutyric acid positive cells in hippocampal field CA1 of the rat. *Neurosci Lett* 278:145–148
- Dolleman-van der Weel MJ, Lopes da Silva FH, Witter MP (1997) Nucleus reuniens thalamic modulates activity in hippocampal field CA1 through excitatory and inhibitory mechanisms. *J Neurosci* 17:5640–5650
- Dolleman-van der Weel MJ, Witter MP (1996) Projections from the nucleus reuniens thalamic to the entorhinal cortex, hippocampal field CA1, and the subiculum in the rat arise from different populations of neurons. *J Comp Neurol* 364:637–650
- Eleore L, López-Ramos JC, Guerra-Narbona R, Delgado-García JM (2011) Role of reuniens nucleus projections to the medial prefrontal cortex and to the hippocampal pyramidal CA1 area in associative learning. *PLoS ONE*. <https://doi.org/10.1371/journal.pone.0023538>
- Fernandez-Ruiz A, Makarov VA, Benito N, Herreras O (2012) Schaffer-specific local field potentials reflect discrete excitatory events

- at gamma frequency that may fire postsynaptic hippocampal CA1 units. *J Neurosci* 32:5165–5176
- Fernandez-Ruiz A, Oliva A, Nagy GA, Maurer AP, Berenyi A, Buzsáki G (2017) Entorhinal-CA3 dual-input control of spike timing in the hippocampus by theta-gamma coupling. *Neuron* 93:1213–1226
- Franklin K, Paxinos G (2008) The mouse brain in stereotaxic coordinates, 3rd edn. Academic Press, San Diego
- Fries P, Nikolic D, Singer W (2007) The gamma cycle. *Trends Neurosci* 30:309–316
- Fung TK, Law C, Leung LS (2016) Associative spike-timing dependent potentiation of the basal dendritic excitatory synapses in the hippocampus in vivo. *J Neurophysiol* 115:3264–3274
- Gonzalez J, Villarreal DM, Morales IS, Derrick BE (2016) Long-term potentiation at temporoammonic path-CA1 synapses in freely moving rats. *Front Neural Circuits* 10:2
- Gugustea R, Tamming RJ, Martin-Kenny N, Bérubé N, Leung LS (2019) Effect of ATRX inactivation on hippocampal synaptic plasticity in mice. *Hippocampus*. <https://doi.org/10.1002/hipo.23174>
- Hajos N, Mody I (1997) Synaptic communication among hippocampal interneurons: properties of spontaneous IPSCs in morphologically identified cells. *J Neurosci* 17:8427–8442
- Hauer BE, Pagliardini S, Dickson CT (2019) The reuniens nucleus of the thalamus has an essential role in coordinating slow-wave activity between neocortex and hippocampus. *ENEURO*.0365-19.2019. <https://doi.org/10.1523/ENEURO.0365-19.2019>
- Herkenham M (1978) The connections of the nucleus reuniens thalami: evidence for a direct thalamo-hippocampal pathway in the rat. *J Comp Neurol* 177:589–609
- Herreras O, Solis JM, del Rio M, Lerma J (1987) Characteristics of activation through the hippocampal trisynaptic pathway in the unanaesthetized rat. *Brain Res* 413:75–86
- Hutchison RM, Chidiac P, Leung LS (2009) Hippocampal long-term potentiation is enhanced in urethane-anesthetized RGS2 knockout mice. *Hippocampus* 19:687–691
- Ito HT, Zhang S-J, Witter MP, Moser EI, Moser MB (2015) A prefrontal-thalamo-hippocampal circuit for goal-directed spatial navigation. *Nature* 522:50–55
- Jefferys JGR, Traub RD, Whittington MA (1996) Neuronal networks for induced ‘40 Hz’ rhythms. *Trends Neurosci* 19:202–208
- Kasyanov AM, Maximov VV, Byzov AL, Berretta N, Sokolov MV, Gasparini S, Cherubini E, Reymann KG, Voronin LL (2000) Differences in amplitude-voltage relations between minimal and composite mossy fibre responses of rat CA3 hippocampal neurons support the existence of intrasynaptic ephaptic feedback in large synapses. *Neuroscience* 101:323–336
- Kay LM, Freeman WJ (1998) Bidirectional processing in the olfactory-limbic axis during olfactory behavior. *Behav Neurosci* 112:541–553
- Klausberger T (2009) GABAergic interneurons targeting dendrites of pyramidal cells in the CA1 area of the hippocampus. *Eur J Neurosci* 30:947–957
- Lasztocki B, Klausberger T (2014) Layer-specific GABAergic control of distinct gamma oscillations in the CA1 hippocampus. *Neuron* 81:1126–1139
- Lasztocki B, Klausberger T (2017) Distinct gamma oscillations in the distal dendritic fields of the dentate gyrus and the CA1 area of mouse hippocampus. *Brain Struct Funct* 222:3355–3365
- Law C, Leung LS (2018) Long-term potentiation and excitability in the hippocampus are modulated differently by theta rhythm. *ENEURO* 2018 5(6):1–25. <https://doi.org/10.1523/ENEURO.0236-18.2018>
- Leung LS (1982) Nonlinear feedback model of neuronal populations in the hippocampal CA1 region. *J Neurophysiol* 47:845–868
- Leung LS (2010) Field potential generation and current source density analysis. In: Vertes RP, Stackman RW (eds) *Electrophysiological recording techniques*, 2nd edn. Humana, Clifton, pp 1–2615
- Leung LS, Fu X-W (1994) Factors affecting paired-pulse facilitation in CA1 neurons in vitro. *Brain Res* 650:75–84
- Leung LS, Lopes da Silva FH, Wadman WJ (1982) Spectral characteristics of the hippocampal EEG in the freely moving rat. *Electroenceph Clin Neurophysiol* 54:203–219
- Leung LS, Peloquin P (2010) Cholinergic modulation differs between basal and apical dendritic excitation of hippocampal CA1 pyramidal cells. *Cereb Cortex* 20:1865–1877
- Leung LS, Peloquin P, Canning KJ (2008) Paired-pulse depression of excitatory postsynaptic current sinks in hippocampal CA1 in vivo. *Hippocampus* 18:1008–1020
- Leung LS, Roth L, Canning KJ (1995) Entorhinal inputs to hippocampal CA1 and dentate gyrus in the rat: a current source-density study. *J Neurophysiol* 73:2392–2403
- Levy WB, Steward O (1979) Synapses as associative memory elements in the hippocampal formation. *Brain Res* 175:233–245
- Lisman JE, Jensen O (2013) The theta-gamma neural code. *Neuron* 77:1002–1016
- Maeda K, Maruyama R, Nagae T, Inoue M, Aonishi T, Miyakawa H (2015) Weak sinusoidal electric fields entrain spontaneous Ca transients in the dendritic tufts of CA1 pyramidal cells in rat hippocampal slice preparations. *PLoS ONE* 10(3):e0122263. <https://doi.org/10.1371/journal.pone.0122263>
- Manabe T, Wyllie DJ, Perkel DJ, Nicoll RA (1993) Modulation of synaptic transmission and long-term potentiation: effects on paired pulse facilitation and EPSC variance in the CA1 region of the hippocampus. *J Neurophysiol* 70:1451–1459
- Mann EO, Radcliffe CA, Paulsen O (2005) Hippocampal gamma-frequency oscillations: from interneurons to pyramidal cells, and back. *J Physiol (Lond)* 562:55–63
- Martin SJ, Grimwood PD, Morris RGM (2000) Synaptic plasticity and memory: an evaluation of the hypothesis. *Ann Rev Neurosci* 23:649–711
- McKenna JT, Vertes RP (2004) Afferent projections to nucleus reuniens of the thalamus. *J Comp Neurol* 480:115–142
- Morales GJ, Ramcharan EJ, Sundararaman N, Morgera SD, Vertes RP (2007) Analysis of the actions of nucleus reuniens and the entorhinal cortex on EEG and evoked population behaviour of the hippocampus. *Conf Proc IEEE Eng Med Biol Soc* 2007:2480–2484
- Nowak LG, Bullier J (1998) Axons, but not cell bodies, are activated by electrical stimulation in cortical gray matter. I. Evidence from chronaxie measurements. *Exp Brain Res* 118:477–488
- Price CJ, Scott R, Rusakov DA, Capogna M (2008) GABAB receptor modulation of feedforward inhibition through hippocampal neurogliaform cells. *J Neurosci* 28:6974–6982
- Rattay F, Paredes LP, Leao RN (2012) Strength-duration relationship for intra-versus extracellular stimulation with microelectrodes. *Neuroscience* 214:1–13
- Remondes M, Schuman EM (2002) Direct cortical input modulates plasticity and spiking in CA1 pyramidal neurons. *Nature* 416:736–740
- Remondes M, Schuman EM (2003) Molecular mechanisms contributing to long-lasting synaptic plasticity at the temporoammonic-CA1 synapse. *Learn Mem* 10:247–252
- Remondes M, Schuman EM (2004) Role for a cortical input to hippocampal area CA1 in the consolidation of long-term memory. *Nature* 431:699–703
- Schulz PE, Cook EP, Johnston D (1994) Changes in paired-pulse facilitation suggest presynaptic involvement in long-term potentiation. *J Neurosci* 14:5325–5337
- Sybirska E, Davachi L, Goldman-Rakic PS (2000) Prominence of direct entorhinal-CA1 pathway activation in sensorimotor and cognitive tasks revealed by 2-DG functional mapping in nonhuman primate. *J Neurosci* 20:5827–5834

- Thomas MJ, Watabe AM, Moody TD, Makhinson M, O'Dell TJ (1998) Postsynaptic complex spike bursting enables the induction of LTP by theta frequency synaptic stimulation. *J Neurosci* 18:7118–7126
- Varela C, Kumar S, Yang JY, Wilson MA (2014) Anatomical substrates for direct interactions between hippocampus, medial prefrontal cortex, and the thalamic nucleus reuniens. *Brain Struct Funct* 219:911–929
- Vertes RP (2006) Interactions among the medial prefrontal cortex, hippocampus and midline thalamus in emotional and cognitive processing in the rat. *Neuroscience* 142:1–20
- Vertes RP, Hoover WB, Do Valle AC, Sherman A, Rodriguez JJ (2006) Efferent projections of reuniens and rhomboid nuclei of the thalamus in the rat. *J Comp Neurol* 499:768–796
- Wang JH, Kelly PT (1997) Attenuation of paired-pulse facilitation associated with synaptic potentiation mediated by postsynaptic mechanisms. *J Neurophysiol* 78:2707–2716
- Witter MP, Groenewegen HJ, Lopes da Silva FH, Lohman AHM (1989) Functional organization of the extrinsic and intrinsic circuitry of the parahippocampal region. *Prog Neurobiol* 33:161–254
- Wouterlood FG (1991) Innervation of entorhinal principal cells by neurons of the nucleus reuniens thalami. anterograde PHA-L tracing combined with retrograde fluorescent tracing and intracellular injection with lucifer yellow in the rat. *Eur J Neurosci* 3:641–647
- Wouterlood FG, Saldana E, Witter MP (1990) Projection from the nucleus reuniens thalami to the hippocampal region: light and electron microscopic tracing study in the rat with the anterograde tracer *Phaseolus vulgaris* leucoagglutinin. *J Comp Neurol* 296:179–203
- Wu LG, Saggau P (1994) Presynaptic calcium is increased during normal synaptic transmission and paired-pulse facilitation, but not in long-term potentiation in area CA1 of hippocampus. *J Neurosci* 14:645–654
- Xu W, Südhof TC (2013) A neural circuit for memory specificity and generalization. *Science* (80-) 339:1290–1295. <https://doi.org/10.1016/j.biotechadv.2011.08.021>
- Yanagihara M, Niimi K, Ono K (1987) Thalamic projections to the hippocampal and entorhinal areas in the cat. *J Comp Neurol* 266:122–141
- Yeckel MF, Berger TW (1990) Feedforward excitation of the hippocampus by afferents from the entorhinal cortex: redefinition of the role of the trisynaptic pathway. *PNAS* 87:5832–5836
- Yeckel MF, Berger TW (1998) Spatial distribution of potentiated synapses in hippocampus: dependence on cellular mechanisms and network properties. *J Neurosci* 18:438–450
- Zucker RS, Regehr WG (2002) Short-term synaptic plasticity. *Ann Rev Physiol* 64:355–405

Publisher's Note Springer Nature remains neutral with regard to jurisdictional claims in published maps and institutional affiliations.